JOURNAL OF GEOPHYSICAL RESEARCH, VOL. 112, D10S23, doi:10.1029/2006JD007579, 2007

Aerosol optical properties along the northeast coast of North America during the New England Air Quality Study–Intercontinental Transport and Chemical Transformation 2004 campaign and the influence of aerosol composition

Wei Wang,[1] Mark J. Rood,[1] Christian M. Carrico,[2] David S. Covert,[3] Patricia K. Quinn,[4] and Timothy S. Bates[4]

Received 30 May 2006; revised 22 January 2007; accepted 9 February 2007; published 23 May 2007.

[1] Optical and hygroscopic properties of submicrometer diameter aerosol particles were measured on board the NOAA R/V *Ronald H. Brown* as part of the NEAQS-ITCT field campaign. The campaign occurred along the northeast coast of North America during the summer of 2004. A scanning relative humidity (RH) nephelometry system (humidograph) measured total light scattering and backscattering coefficients (σ_{sp} and σ_{bsp}, respectively) at three wavelengths (λs) and RH = 26% and while RH was scanned between 40% and 85%. These measurements were combined with aerosol light absorption and composition measurements to describe σ_{sp}, σ_{bsp}, single scattering albedo (ω), Ångström exponent ($å$), and hemispheric backscatter fraction (b) at a low reference RH of 26 ± 4% and the aerosol's hygroscopic properties based on its optical response up to 85% RH. Humidogram curve structure was dominated by hygroscopic growth without hysteresis (76% frequency). Dependence of the aerosol's σ_{sp} values with changes in RH, $f_{\sigma sp}$(RH, 26), was observed to decrease with increasing mass fraction of particulate organic matter (POM, F_O). Statistical analyses indicated that increasing F_O resulted in a less hygroscopic aerosol, while increasing molar equivalence ratio (ER) resulted in lower hysteresis factors based on the aerosols' optical responses at a 0.95 confidence level. ω showed little RH dependence while $å$ and b decreased with increasing RH values. Values for $å(\lambda_1, \lambda_2)$, b, and $f_{\sigma sp}$(82, 26) increased with increasing λ values. Sensitivities of top of the atmosphere aerosol radiative forcing to changes in ω, b, and σ_{sp} with RH were also estimated.

Citation: Wang, W., M. J. Rood, C. M. Carrico, D. S. Covert, P. K. Quinn, and T. S. Bates (2007), Aerosol optical properties along the northeast coast of North America during the New England Air Quality Study–Intercontinental Transport and Chemical Transformation 2004 campaign and the influence of aerosol composition, *J. Geophys. Res.*, *112*, D10S23, doi:10.1029/2006JD007579.

1. Introduction

1.1. Scientific Motivation and Objectives

[2] Atmospheric aerosol particles affect the Earth's radiative energy balance directly by scattering and absorbing sunlight [*Charlson et al.*, 1992; *Ramanathan and Vogelmann*, 1997], and indirectly by acting as cloud condensation nuclei (CCN, see Notation), thereby influencing cloud albedo [*Twomey*, 1991], cloud lifetime [*Albrecht*, 1989], precipitation patterns [*Rosenfeld*, 2000] and precipitation distributions [*Ramanathan et al.*, 2001a]. Natural aerosols have been perturbed by anthropogenic activities in many regions of the Earth by increasing atmospheric concentrations of sulfate, nitrate, organic compounds, soot, and dust. The global estimate of aerosol direct radiative forcing from satellite measurements gives a clear-sky annual average of -1.9 W m^{-2} with a standard deviation of 0.3 W m^{-2} [*Bellouin et al.*, 2005]. The indirect effect of anthropogenic aerosol is estimated within the range of 0 to -2 W m^{-2} [*Lohmann and Feichter*, 2005]. These values are comparable to current greenhouse gas forcing estimates of +2.43 W m^{-2} [*Houghton et al.*, 2001]. Aerosol concentrations are particularly high in regions downwind of sources where diurnally averaged clear-sky surface forcing can reach +30 W m^{-2} [*Russell et al.*, 1999a; *Ramanathan et al.*, 2001a]. This uneven forcing has the potential to cause regional-scale to hemispheric-scale effects on climate patterns.

[1]Department of Civil and Environmental Engineering, University of Illinois, Urbana, Illinois, USA.
[2]Department of Atmospheric Science, Colorado State University, Fort Collins, Colorado, USA.
[3]Department of Atmospheric Sciences, University of Washington, Seattle, Washington, USA.
[4]Pacific Marine Environmental Laboratory, NOAA, Seattle, Washington, USA.

0148-0227/07/2006JD007579$09.00

[3] International field campaigns during the past decade have studied properties of natural and anthropogenically perturbed aerosols and their effects on radiative transfer in background marine conditions (ACE-1) [*Bates et al.*, 1998], downwind of North America (TARFOX) [*Russell et al.*, 1999b], Europe (ACE-2) [*Raes et al.*, 2000], India (INDOEX) [*Ramanathan et al.*, 2001b], and Asia (ACE-Asia) [*Huebert et al.*, 2003]. Results from these experiments have been used to develop and refine three-dimensional chemical transport models (CTMs) and radiative transfer models (RTMs) that evaluate perturbations to Earth's radiative-energy balance by anthropogenic aerosol particles [*Charlson et al.*, 1992; *Kiehl et al.*, 2000; *Anderson et al.*, 2003; *Chin et al.*, 2004; *Takemura et al.*, 2005]. Results from these models are compelling, but parameterizations used in these models need to be improved to decrease the uncertainties in the model results.

1.2. Hygroscopicity and Radiative Forcing

[4] The sensitivity of climate forcing to realistic variations in sulfate aerosol size and ammonium to sulfate molar ratio was estimated to be ±20% [*Boucher and Anderson*, 1995]. Such sensitivity was attributed to a number of compensating factors that link the following three aerosol optical parameters: the light scattering efficiency per unit sulfate mass at RH values below 50%, the ratio of backscatter to total scatter, and the increase in light scattering as a function of RH [*Charlson et al.*, 1991]. *Boucher and Anderson* [1995] concluded that these optical parameters should not be treated independently in either theoretical or experimental investigations of direct climate forcing, and that the high RH backscattering efficiency is a logical focus for research on local aerosol optical properties as they relate to direct climate forcing.

[5] It has been observed for continentally polluted air masses that the hygroscopic growth in particle diameter (d_p) is smaller than expected for an entirely soluble particle composed of a mixture of the major inorganic ions observed in the bulk aerosol and this smaller hygroscopic growth was attributed to a hygroscopically inactive volume fraction of about 0.50 [*Swietlicki et al.*, 1999]. Aerosol laboratory studies demonstrated that select carboxylic acids and alkanes decreased the amount of hygroscopic growth in d_p when those compounds replaced the inorganic compounds (i.e., NaCl and $(NH_4)_2SO_4$) at the same initial d_p [*Choi and Chan*, 2002; *Hansson et al.*, 1998]. Reductions in the hygroscopic growth of d_p were also shown to occur with increasing mass fraction of organic material for aerosols generated during biomass burning [*Carrico et al.*, 2005; *Malm et al.*, 2005]. Similarly, it is important to evaluate the influence of organic material and RH on an ambient aerosol's optical properties at a number of geographical locations that have different aerosol sources.

[6] The primary objective of this research is to quantify the optical and hygroscopic properties of ambient aerosol in the marine boundary layer along the northeast coast of North America and the influence of aerosol chemistry on these properties. Aerosol particle parameters directly measured here include the total light scattering coefficient (σ_{sp}), the hemispheric backscatter coefficient (σ_{bsp}), and the light absorption coefficient (σ_{ap}) at three visible wavelengths. The light extinction coefficient (σ_{ep}) is the sum of σ_{sp} and σ_{ap}. The hemispheric backscatter fraction ($b = \sigma_{bsp}/\sigma_{sp}$) is the fraction of the scattered light that is scattered into the backward hemisphere [*Marshall et al.*, 1995] and is related to the fraction that is redirected upward from the Earth. Single scattering albedo ($\omega = \sigma_{sp}/\sigma_{ep}$) is fundamental to determining the aerosols' ability to cause Earth-atmosphere cooling (scattering) versus warming (absorption) at a given surface albedo [*Heintzenberg et al.*, 1997; *Russell et al.*, 2002]. The Ångström exponent ($\mathring{a}$) is a measure of the wavelength dependence of light scattering [*Ångström*, 1964] approximated by equation (1) with σ_{sp} values at a given RH for discrete values of λ_1 and λ_2, and is likewise defined for σ_{bsp}:

$$\mathring{a} \equiv -\frac{\log\left(\sigma_{sp,\lambda_1}/\sigma_{sp,\lambda_2}\right)}{\log(\lambda_1/\lambda_2)} \tag{1}$$

[7] Aerosol hygroscopic response with respect to σ_{sp} is described by $f_{\sigma sp}(\mathrm{RH}, \mathrm{RH_{ref}})$, which is the ratio of σ_{sp} at a given RH to σ_{sp} at a low reference RH ($\mathrm{RH_{ref}}$). Likewise, $f_{\sigma bsp}(\mathrm{RH}, 26)$ is defined for σ_{bsp} values. The hysteresis factor ($h(\mathrm{RH})$) is defined as the ratio of σ_{sp} on the upper branch to σ_{sp} on the lower branch of the hysteresis loop at the specified RH to quantify the importance of hysteresis to an aerosol's optical properties.

2. Methodology

2.1. Scanning Relative Humidity Nephelometry

[8] An in situ scanning-RH nephelometry system (humidograph) was used to measure aerosol light scattering coefficients at three wavelengths (450 nm, 550 nm, and 700 nm) as RH was scanned under increasing and decreasing RH conditions. The humidograph was first developed by *Pilat and Charlson* [1966] and then improved and implemented by *Covert et al.* [1972], *Charlson et al.* [1974], *Larson et al.* [1982], *Weiss et al.* [1983], *Rood et al.* [1985, 1987a, 1987b, 1989], *Ruby et al.* [1989], *Koloutsou-Vakakis et al.* [2001], and *Carrico et al.* [1998, 2000, 2003]. The nephelometry system used here was described in detail by *Carrico et al.* [2003]. A description of modifications that were made to the humidograph in preparation for the NEAQS-ITCT 2004 field campaign is provided here as well as a brief description of the system (Figure 1). The humidograph was repackaged to reduce its volume by 30% because of space restrictions on the ship. The 50% upper aerodynamic cutoff d_p at the humidograph's inlet was kept constant at 1 μm and at 60% RH instead of switching between 1 μm and 10 μm inlets. Temperature (T) control was improved by increasing the ventilation within the humidograph's enclosure.

[9] The average ambient air temperature and RH during the field campaign were 17.3 ± 2.5°C and 90 ± 10% RH, respectively (given as the arithmetic mean ± one standard deviation). Standard deviations represent the variability in the measured or derived parameters that are not explicitly due to measurement errors or propagated uncertainties. By heating the sample, the aerosol was thermally dried to 60 ± 3% RH in a community sampling inlet before passing through an impactor with a 50% upper aerodynamic cutoff d_p of 1 μm. The inlet was located 18 m above sea level and

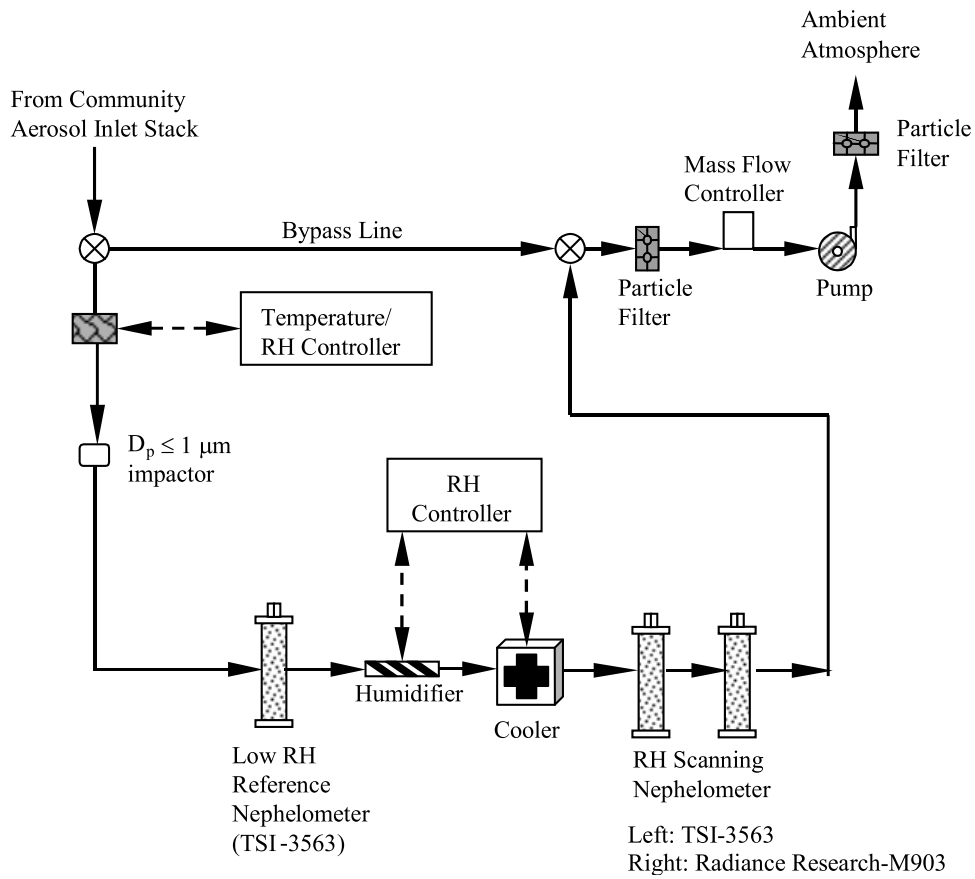

Figure 1. Scanning RH nephelometry system deployed during NEAQS-ITCT 2004.

forward of the ship's exhaust stack, and was automatically rotated into the wind to reduce particle loss and minimize potential ship contamination [*Bates et al.*, 2002]. The aerosol was then dried to an RH = RH_{ref} of 26 ± 4% by heating the sample to 37 ± 1°C before the low RH reference σ_{sp} and σ_{bsp} values were measured in an integrating nephelometer (TSI Inc., Model 3563). The power to the lamps that illuminate the scattering volume in each of the TSI nephelometers was set at 50 W. The aerosol's RH was then controlled by adding water vapor (custom Teflon membrane humidifier) or by changing sample dry bulb temperature (Peltier thermoelectric coolers, Melcor, Inc.) downstream of the low RH reference nephelometer. The aerosol then passed through two nephelometers (TSI Inc., Model 3563 and Radiance Research (RR), Model M903) that were operated in series with increasing or decreasing RH conditions that ranged from 40 ± 3% RH to 85 ± 5% RH. The humidification system allowed for (1) increasing RH scans starting with aerosol assumed to be "dry" or to have minimal water content and (2) decreasing RH scans starting with aerosol assumed to be "hydrated" by controlling the temperature and the amount of water vapor added to the aerosol upstream of the second nephelometer. This arrangement allowed for the detection of hysteresis and the formation of metastable droplets in the scanning-RH nephelometers. The RH in the scanning-RH nephelometers was held at the constant low RH = 40% for 10 min, scanned to the high RH = 85% over 15 min, held at the high RH for 10 min, and then scanned down to the low RH condition over 15 min. This sequence was followed by a 20-min period when the nephelometers were first zeroed with particle free air (5 min) and then set on standby (15 min) until a constant low RH was achieved for the next RH scan. Humidograms were then generated that describe an aerosol's optical property measured at a controlled RH condition divided by that optical property measured at a low RH_{ref} condition (e.g., $f_{\sigma sp}(RH, RH_{ref})$ for σ_{sp}).

[10] RH and dry bulb temperatures of the scanning-RH nephelometers were measured with sensors at the inlet and near the sensing volume of each nephelometer [*Carrico et al.*, 2003]. Heating of the walls surrounding the sensing volume by the scanning-RH nephelometers' lamps caused the RH that was measured immediately upstream of the RH-scanning nephelometers to be greater than the nephelometers' internally measured "sensing volume RH" values. The temperature of the TSI scanning RH nephelometer's sensing volume was at 33.3 ± 1.9°C to minimize instrumental heating effects on sample RH, and to limit losses of semivolatile species [*ten Brink et al.*, 2000]. The protocols that were used to calculate "sensing volume RH" from the measured T and RH values that are reported here are described by *Carrico et al.* [2003].

2.2. Continuous Light Scattering Measurement at Constant Intermediate RH

[11] A fourth nephelometer (TSI Inc., Model 3563) was operated by the National Oceanic and Atmospheric

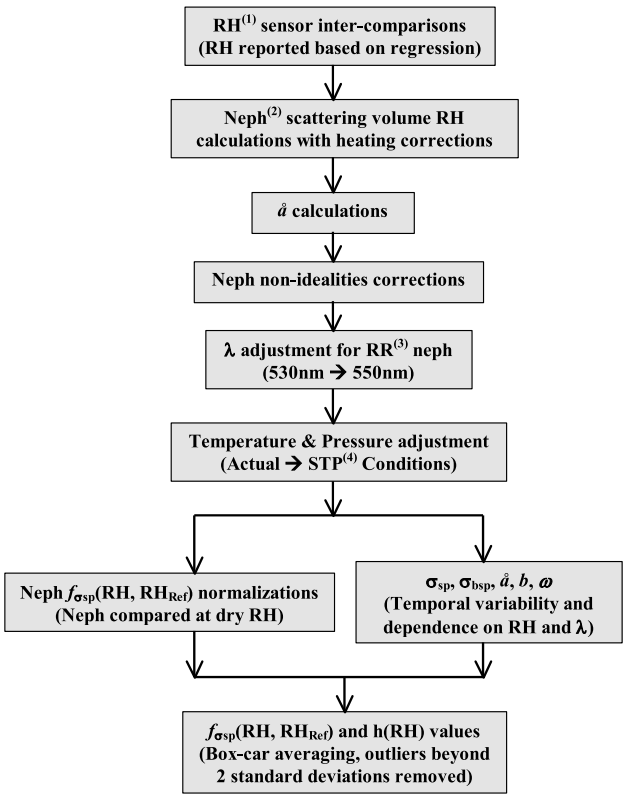

(1) RH – Relative humidity;

(2) Neph – Nephelometer;

(3) RR – Radiance Research (nephelometer);

(4) STP – Standard temperature and pressure, T = 0°C and P = 101.3 kPa.

Figure 2. Flowchart of data reduction and corrections.

Administration–Pacific Marine Environment Laboratory (NOAA-PMEL) in parallel to the humidograph to provide continuous σ_{sp} and σ_{bsp} measurements at RH = 60 ± 3%. This was accomplished by heating of the sample so that the aerosol only experienced decreasing RH conditions to a mean RH of 60% (RH = $60_{decrease}$) as it passed from the outside ambient environment (17.3 ± 2.5°C and 90 ± 10% RH) to the nephelometer. The high ambient RH value and the intermediate sample RH in this nephelometer allows the aerosol to remain hydrated because 60% RH is above the crystallization relative humidity (CRH) of most chemical species observed in sampled aerosol [*Tang et al.*, 1995; *Kus et al.*, 2004; *Shaw and Rood*, 1990]. The aerosols' hydration state can be obtained by comparing the light scattering data from NOAA-PMEL's nephelometer that are normalized with light scattering data obtained from the humidograph's RH_{ref} nephelometer ($f_{\sigma sp}(60_{decrease}, 26)$) with $f_{\sigma sp}(60, 26)$ values from the humidograph that describe the lower branch of the hysteresis loop to determine if the aerosol is located on the upper branch, on the lower branch, or between the two branches of the aerosol's hysteresis loop. Optical properties of the ambient aerosol including $\sigma_{sp}(RH_{ambient})$ and $\omega(RH_{ambient})$ can be determined with $f_{\sigma sp}(RH_{ambient}, 26)$ values, the corresponding low RH σ_{sp} and σ_{ap} values, and knowledge of the ambient aerosols' hydration state.

2.3. Single Scattering Albedo and Chemical Speciation

[12] The light absorption coefficient for submicrometer diameter aerosols, with a 50% upper aerodynamic cutoff d_p of 1 μm, was derived from a particle soot absorption photometer (PSAP, Radiance Research Inc.) that operated at λ = 467 nm, 530 nm, and 660 nm, and RH <25% [*Bond et al.*, 1999; *Virkkula et al.*, 2005]. The following discussion pertains to σ_{sp} and σ_{ap} at λ = 550 nm, unless otherwise specified. The values of σ_{ap} are assumed to be only weakly dependent on RH [e.g., *Redemann et al.*, 2001] and assumed constant for RH conditions reported here when calculating ω. In this study, ω at λ = 550 nm was determined from simultaneously measured σ_{sp} values obtained from the humidograph's low RH reference nephelometer and σ_{ap} values from the PSAP measurements that were adjusted to 550 nm on the basis of equation (1) where σ_{sp} was replaced by σ_{ap}.

[13] Particle number-size distributions in the diameter range of 0.020 μm to 0.8 μm Stokes diameter at 60% RH were determined using a twin differential mobility particle sizer (DMPS) [*Bates et al.*, 2005]. The aerosol's nonrefractory (NR) chemical composition was measured with an Aerodyne Aerosol Mass Spectrometer (AMS) [*Quinn and Bates*, 2005]. Reported aerosol chemical properties that are of interest to this study include (1) mass fraction of particulate organic matter (POM, $F_O = \frac{mass_{NR-POM}}{mass_{NR-POM} + mass_{NR-SO_4^{2-}}}$) and (2) acidity, as described by the molar equivalence ratio with respect to ammonium, nitrate, and sulfate (ER = $\frac{mole_{NH_4^+}}{mole_{NO_3^-} + 2\ mole_{SO_4^{2-}}}$) [*Quinn et al.*, 2006].

2.4. Data Reduction and Analysis

[14] The raw data were adjusted to relevant aerosol optical properties as outlined in the data reduction flowchart (Figure 2). Light scattering values from the three TSI nephelometers were corrected for nonidealities as a function of RH with measured values of *å*(RH) [*Anderson and Ogren*, 1998; *Carrico et al.*, 2000, 2003]. Light scattering values from the RR nephelometer were also corrected for nonidealities using the same correction factors that were used for the TSI nephelometer, and the scattering values were adjusted from its instrumental λ = 530 nm to λ = 550 nm using *å*(RH) values from the TSI scanning-RH nephelometer. Temperature and pressure measurements from the TSI and RR nephelometers were used to adjust the reported optical measurements to standard temperature and pressure (STP) of 0°C and 101.3 kPa. Values for σ_{sp} and σ_{bsp} that were obtained from the RH-scanning nephelometers were normalized to their corresponding values from the upstream low RH reference nephelometer during periods of constant low RH. This normalization was done to account for operating differences such as modest particle losses, calibration differences, and RH conditions between the nephelometers [*Carrico et al.*, 2003]. Values for "dry" σ_{sp} and σ_{bsp} from the TSI RH-scanning nephelometer before normalization were 2% lower to 3% higher and 4% to 10% higher at all λs when compared to equivalent values from the TSI low RH reference nephelometer, respectively. "Dry" σ_{sp} values from the RR RH-scanning nephelometer were 2% lower at λ = 550 nm when compared to equivalent values from the TSI low RH reference nephelometer before

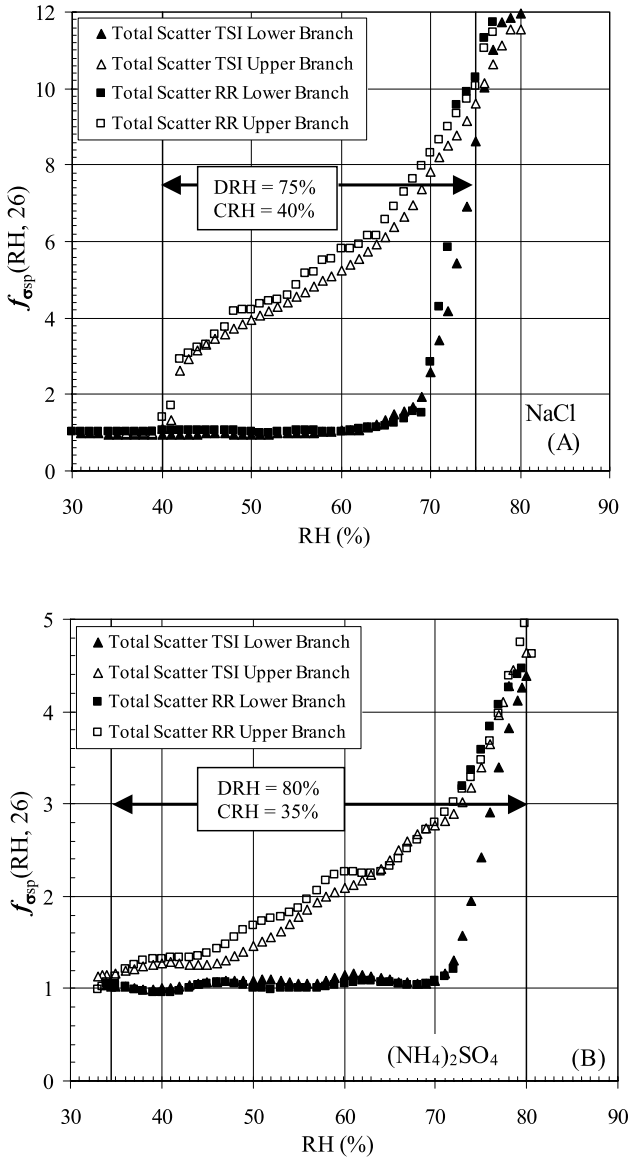

Figure 3. Measurements of $f_{\sigma sp}$(RH, 26) with the TSI and Radiance Research (RR) instruments during the field campaign with test aerosols (a) NaCl and (b) $(NH_4)_2SO_4$.

normalization. Boxcar averages over 4% RH ranges were calculated and centered at every 1% RH value for the $f_{\sigma sp}$(RH, 26) curves. Outliers beyond ±2 standard deviations of the mean values at each RH range, which consisted of <5% of the data set, were removed from the raw data set.

[15] During the field campaign, four humidogram curve structures were apparent: structure A, less hygroscopic; structure B, hygroscopic, nondeliquescent and without hysteresis; structure C, hygroscopic, nondeliquescent and with hysteresis; and structure D, hygroscopic and deliquescent. The ambient humidograms were classified on the basis of their curve structures as follows: structure A, less hygroscopic, with $f_{\sigma sp}(82, 26) \leq 1.40$; structure B, hygroscopic, nondeliquescent without hysteresis, with $f_{\sigma sp}(82, 26) > 1.40$ and $f_{\sigma sp}$(RH, 26) values on the lower and upper branches differing ≤5%; structure C, hygroscopic, nondeliquescent with hysteresis, $f_{\sigma sp}(82, 26)$ values > 1.40 and $f_{\sigma sp}$(RH, 26) values on the lower and upper branches differing > 5%; and structure D, hygroscopic and deliquescent, with $f_{\sigma sp}(82, 26)$ values > 1.40 and $f_{\sigma sp}$(RH, 26) values on the lower branch increasing ≥50% over the RH range 60% to 85%.

[16] Measured $f_{\sigma sp}$(RH, 26) values were then fit with empirical monotonic curve structures A and B (equation (2)).

$$f(RH) = 1 + a\left(\frac{RH}{100}\right)^b \tag{2}$$

Curve structure C has separate curve fits for the lower and upper branches of the hysteresis loop as shown in equations (3) and (4), respectively,

$$f(RH) = a \times \left(\frac{RH}{100}\right)^4 + b \times \left(\frac{RH}{100}\right)^3 + c \times \left(\frac{RH}{100}\right)^2 + g \times \left(\frac{RH}{100}\right) + k \tag{3}$$

$$f(RH) = c\left(1 - \frac{RH}{100}\right)^{-g} \tag{4}$$

A fourth-order polynomial equation was chosen to best describe the lower branch of this hysteresis curve structure because there was no observed deliquescence step. The magnitude of any step change in light scattering that was attributed to deliquescence was typically smaller than those observed during ACE-Asia [*Carrico et al.*, 2003].

[17] The absolute relative difference (ARD) is used as a statistical measure to compare the difference between two relevant properties and is defined by:

$$\mathrm{ARD} = \frac{1}{n}\sum_{i=1}^{n}\left[\frac{|y_i^{(1)} - y_i^{(2)}|}{y_i^{(1)}} \times 100\right] \tag{5}$$

where n is the number of data points, and $y^{(1)}$ and $y^{(2)}$ represent properties of interest. For example, $y^{(1)}$ and $y^{(2)}$ could be σ_{sp} values obtained from the TSI and RR scanning-RH nephelometers, respectively.

[18] Multiple and single linear regressions were performed to investigate the effects of the aerosol chemistry (F_O and ER) on its hygroscopicity ($f_{\sigma sp}(82, 26)$) and hysteresis factor ($h(60)$). The multiple linear regression equation takes the form of

$$y = \beta_0 + \beta_1 F_O + \beta_2 \mathrm{ER} \tag{6}$$

where y is $f_{\sigma sp}(82, 26)$ or $h(60)$; β_0 is a constant, where the regression line intercepts the ordinate; and β_1 and β_2 are the regression coefficients, representing the amount y changes when the corresponding values of F_O or ER change 1 unit [*Fox*, 1997]. The significance of F_O and ER is assessed with the t-test, where t is the parameter estimate divided by its standard deviation, and p-value is the probability of wrongly rejecting the null hypothesis if it is in fact true. The result is considered significant if the p-value is less than

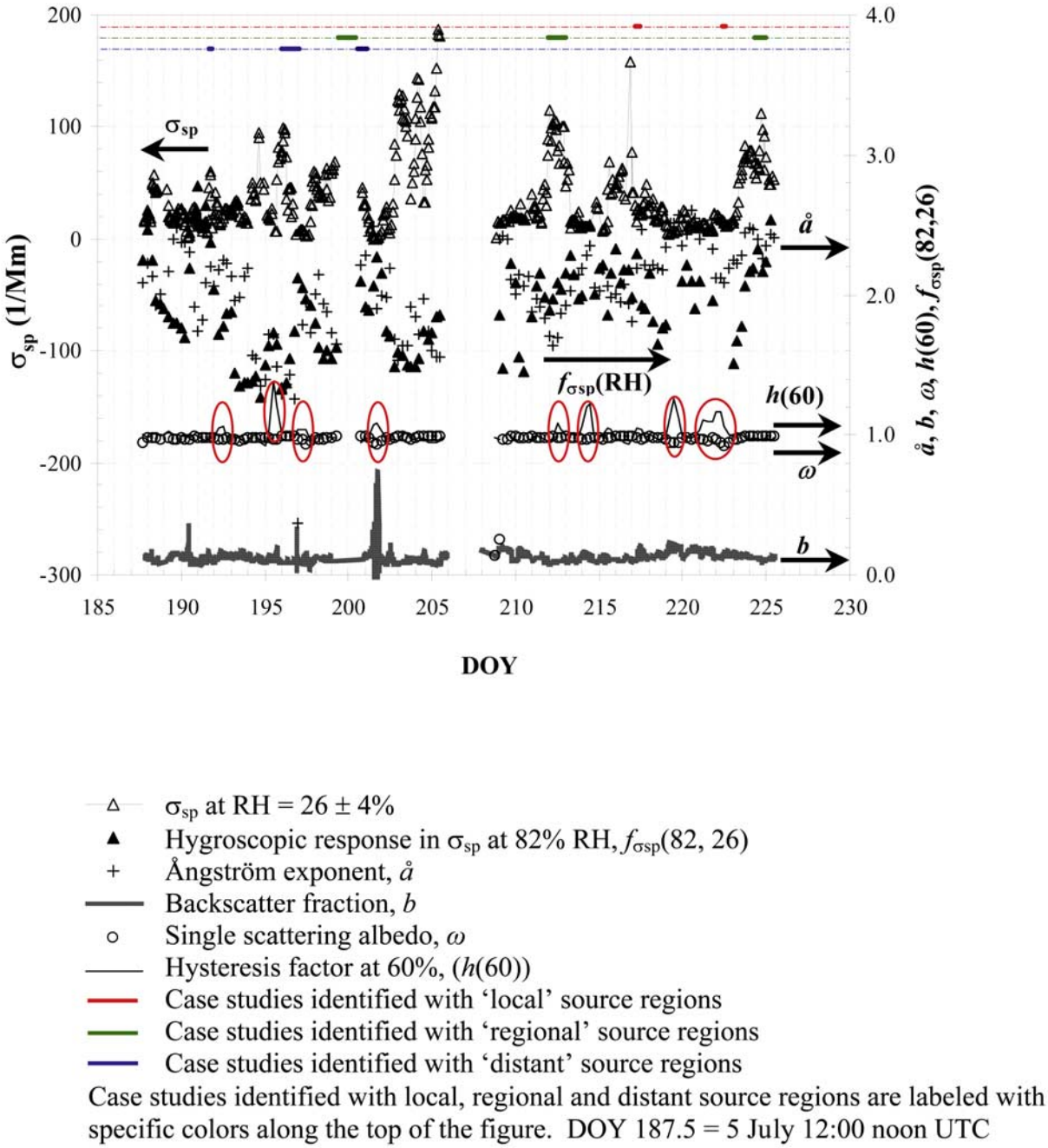

Figure 4. Temporal variability of the optical properties: total light scattering coefficient, σ_{sp}, measured at $\lambda = 550$ nm at RH = 26 ± 4%; hysteresis factor at 60%, $h(60)$; Ångström exponent, $å$ at low RH for $\lambda =$ 450 and 550 nm; backscatter ratio, b, and single scattering albedo, ω, at λ = 550 nm and low RH condition; and hygroscopic response in σ_{sp} at RH = 82%, $f_{\sigma sp}(82, 26)$.

one minus the significance level (0.95) (i.e., 1 − 0.95 = 0.05). Small *p*-values suggest that the null hypothesis is unlikely to be true.

3. Results and Discussion

3.1. Calibrations and Quality Control

[19] There were 573 ambient humidograms generated during the field campaign, of which 529 humidograms yielded curve fits according to equations (2)–(4). The 44 humidograms that were excluded from the analyses either had unstable/unsuccessful RH control, or were obtained during fog periods when the signal-to-noise ratio was too low to yield statistically significant curve fits. Additional calibrations and instrument repairs resulted in the humidograph measuring aerosol properties during 90% of the field campaign.

[20] Leak tests, calibrations and monitoring procedures were completed during the cruise to check the measured values. Leak tests on the humidograph were completed at the beginning and end of both sections of the field campaign. Total scattering values of particle free air after subtraction of Rayleigh scattering values were, on average, 0.5% of the ambient σ_{sp} value, indicating negligible leaks in the system. Simultaneous calibration of the humidograph's nephelometers occurred six times on a weekly basis using dry filtered air and CO_2. The TSI and RR nephelometers were also zeroed with filtered air before each increasing RH scan. The calibrations for the two humidograph nephelometers were stable throughout the experiment with the relative standard deviations (standard deviation divided by the mean) of the calibration factors for total scatter and back scatter ranging from 0.6% to 6.3% and 0.8% to 6.2%, respectively, for at all three λs during the field campaign. Weekly calibrations of the RR nephelometer with CO_2 showed that the light scattering coefficient for CO_2 was 21.2 ± 0.9 Mm^{-1}, which was within 5.1% of the calibration value for CO_2 (21.4 Mm^{-1}) at the same conditions of 530 nm, 293 K, and 101.3 kPa. The ARD between σ_{sp} values obtained from the two scanning-RH nephelometers was within 2% at all controlled RH conditions during the field campaign before normalizing those σ_{sp} values with the corresponding σ_{sp} values from the low RH reference nephelometer. This agreement suggests that instrumental differences (e.g., sample heating, light source differences, and truncation angles) did not cause significant artifacts between the nephelometers' σ_{sp} measurements at controlled RH conditions.

[21] Humidograms, that describe $f_{\sigma sp}$(RH, 26) as a function of the nephelometer's sample RH, were also generated with reagent-grade test aerosol to evaluate the performance of the system before, during, and after the field campaign. Test aerosols were generated by bubbling filtered air through aqueous solutions that contained reagent grade NaCl or $(NH_4)_2SO_4$ and mixing the resulting aerosol with particle-free air to yield nominal σ_{sp} values of 25 Mm^{-1}. The resulting test aerosols' humidograms were then generated in the same manner as for the ambient aerosol. The test aerosol revealed deliquescent relative humidity (DRH) and CRH values of $74.6 \pm 2.0\%$ and $40.2 \pm 2.2\%$ for NaCl, and $79.8 \pm 1.3\%$ and $34.5 \pm 0.7\%$ for $(NH_4)_2SO_4$, respectively (Figure 3). Published values of DRH and CRH at 25°C include 75% and 42–43% for NaCl and 79% and 36–40% for $(NH_4)_2SO_4$, respectively [*Tang*, 1980; *Tang and Munkelwitz*, 1993].

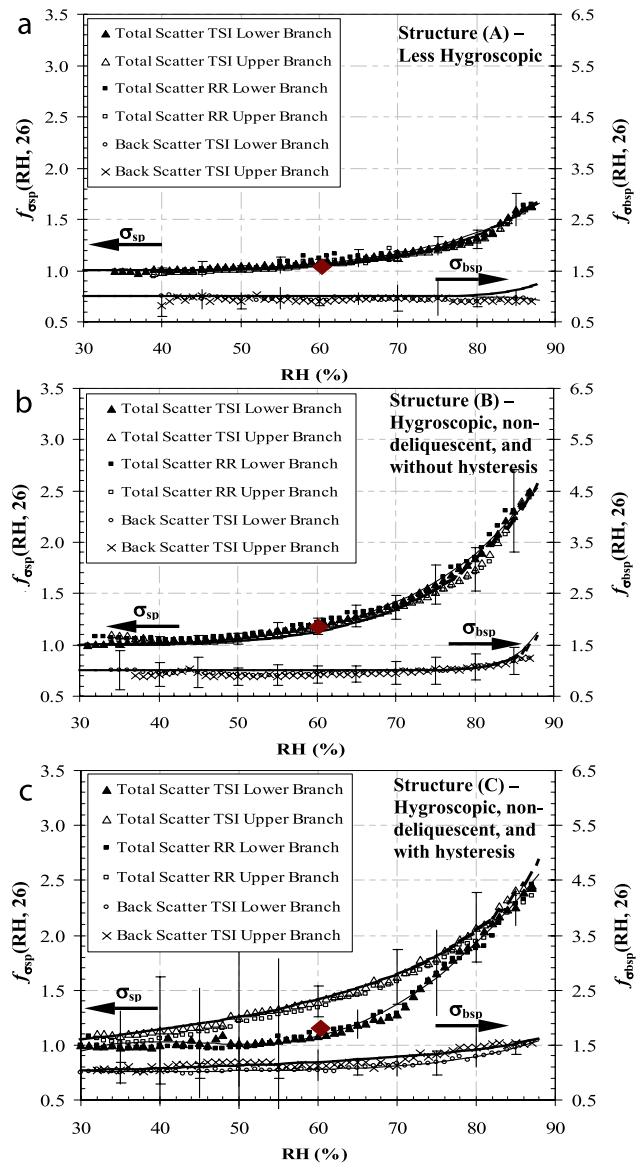

Figure 5. Humidogram curve structures observed during field campaign. Large diamond symbol describes $f_{\sigma sp}(60_{decrease}, 26)$. Standard deviations are provided as vertical lines. (a) Less hygroscopic; (b) hygroscopic, nondeliquescent and without hysteresis; and (c) hygroscopic, nondeliquescent and with hysteresis.

3.2. Overview of Aerosol Optical Properties During NEAQS-ITCT 2004

[22] The following discussion pertains to the entire field campaign with $d_p \leq 1$ μm, sample RH = 26 ± 4%, and λ = 550 nm, unless otherwise specified (Figure 4). Fifteen minute averaged σ_{sp} values were 42.9 ± 35.2 Mm^{-1} and ranged from 0.45 to 193 Mm^{-1}. Hygroscopic response in σ_{sp} at RH = 82%, $f_{\sigma sp}$(82, 26), was 1.88 ± 0.39. The hysteresis factor at 60% RH, *h*(60), was relatively constant at 1.02 ± 0.07. Values of *h*(60) greater than 1.05 are

Less Hygroscopic	Total Scattering	$f_{\sigma_{sp}}$(RH, 26) (450 nm)				$f_{\sigma_{sp}}$(RH, 26) (550 nm)				$f_{\sigma_{sp}}$(RH, 26) (700 nm)			
		A	b	$f_{\sigma_{sp}}$(82, 26)	R^2	a	b	$f_{\sigma_{sp}}$(82, 26)	R^2	a	b	$f_{\sigma_{sp}}$(82, 26)	R^2
		1.19	5.31	1.36 ± 0.10	0.991	1.41	5.98	1.38 ± 0.10	0.992	1.76	8.08	1.36 ± 0.15	0.993
	Back Scattering	$f_{\sigma_{bsp}}$(RH, 26) (450 nm)				$f_{\sigma_{bsp}}$(RH, 26) (550 nm)				$f_{\sigma_{bsp}}$(RH, 26) (700 nm)			
		A	b	$f_{\sigma_{bsp}}$(82, 26)	R^2	a	b	$f_{\sigma_{bsp}}$(82, 26)	R^2	a	b	$f_{\sigma_{bsp}}$(82, 26)	R^2
		9.06	22.93	0.97 ± 0.10	0.608	-1.83	24.71	0.94 ± 0.11	0.633	0.49	0.91	1.35 ± 0.52	0.664
Hygroscopic, non-deliquescent and without hysteresis	Total Scattering	$f_{\sigma_{sp}}$(RH, 26) (450 nm)				$f_{\sigma_{sp}}$(RH, 26) (550 nm)				$f_{\sigma_{sp}}$(RH, 26) (700 nm)			
		A	b	$f_{\sigma_{sp}}$(82, 26)	R^2	a	b	$f_{\sigma_{sp}}$(82, 26)	R^2	a	b	$f_{\sigma_{sp}}$(82, 26)	R^2
		2.68	5.78	1.80 ± 0.28	0.998	3.18	5.71	1.98 ± 0.31	0.998	2.91	6.49	1.87 ± 0.39	0.998
	Back Scattering	$f_{\sigma_{bsp}}$(RH, 26) (450 nm)				$f_{\sigma_{bsp}}$(RH, 26) (550 nm)				$f_{\sigma_{bsp}}$(RH, 26) (700 nm)			
		A	b	$f_{\sigma_{bsp}}$(82, 26)	R^2	a	b	$f_{\sigma_{bsp}}$(82, 26)	R^2	a	b	$f_{\sigma_{bsp}}$(82, 26)	R^2
		0.96	5.07	1.24 ± 0.27	0.948	26.26	27.85	1.08 ± 0.26	0.868	8.12	21.84	1.14 ± 0.39	0.680
Hygroscopic, non-deliquescent, with hysteresis (Upper branch)	Total Scattering	$f_{\sigma_{sp}}$(RH, 26) (450 nm)				$f_{\sigma_{sp}}$(RH, 26) (550 nm)				$f_{\sigma_{sp}}$(RH, 26) (700 nm)			
		C	g	$f_{\sigma_{sp}}$(82, 26)	R^2	c	g	$f_{\sigma_{sp}}$(82, 26)	R^2	c	g	$f_{\sigma_{sp}}$(82, 26)	R^2
		0.86	0.55	2.24 ± 0.32	0.996	0.87	0.53	2.14 ± 0.40	0.998	0.77	0.57	2.08 ± 0.89	0.990
	Back Scattering	$f_{\sigma_{bsp}}$(RH, 26) (450 nm)				$f_{\sigma_{bsp}}$(RH, 26) (550 nm)				$f_{\sigma_{bsp}}$(RH, 26) (700 nm)			
		C	g	$f_{\sigma_{bsp}}$(82, 26)	R^2	c	g	$f_{\sigma_{bsp}}$(82, 26)	R^2	c	g	$f_{\sigma_{bsp}}$(82, 26)	R^2
		1.05	0.15	1.38 ± 0.15	0.864	0.95	0.25	1.52 ± 0.32	0.921	1.01	0.17	1.35 ± 0.58	0.943
Hygroscopic, non-deliquescent, with hysteresis (Lower branch)	wavelength	$f_{\sigma_{sp}}$(RH, 26)							$f_{\sigma_{bsp}}$(RH, 26)						
	(λ)	A	b	c	g	k	$f_{\sigma_{sp}}$(82, 26)	R^2	a	b	c	g	k	$f_{\sigma_{bsp}}$(82, 26)	R^2
	450 nm	-43.5	114	-100	36.2	-3.6	2.17 ± 0.15	0.994	1.39	0.62	-2.81	1.79	0.70	1.25 ± 0.15	0.962
	550 nm	-31.2	89.5	-82.4	30.8	-3.1	2.11 ± 0.17	0.997	17.8	-34.6	25.7	-8.44	2.04	1.36 ± 0.26	0.986
	700nm	-16.7	59.8	60.9	24.5	-2.4	1.96 ± 2.14	0.995	4.89	-5.80	1.64	0.31	0.92	1.27 ± 0.07	0.959

*a and b for both lower and upper branches of (1) Less hygroscopic and (2) Hygroscopic without hysteresis using equation 2; a, b, c, g, and k for lower branches and c and g for upper branches of (3) Hygroscopic with hysteresis using equation 3 and 4, respectively, and averaged hygroscopic response factor at RH = 82% ($f_{\sigma_{sp}}$(82, 26)) and R^2 for the fits are also given.

Figure 6. Curve fit parameters for f(RH, 26) for σ_{sp} and σ_{bsp}, measured at λ = 450, 550, and 700 nm with particle diameter upper size cut of $d_p \leq 1$ μm.

highlighted in the ovals in Figure 4. They occurred 12% of the time and correspond to humidogram curve structures C and D, where hysteresis was observed. Values of ω and b for the entire field campaign were 0.92 ± 0.06 and 0.12 ± 0.02, respectively. The Ångström exponent, $å$, for λ = 450 and 550 nm was $å$ = 2.1 ± 0.3. The results for $å$ are largely determined by the aerosol inlet to the humidograph, which had a 50% upper aerodynamic cutoff d_p of 1 μm. However, this value can be used as a reference to changes in $å$ values due to changes in RH values as discussed later.

3.3. Humidogram Curve Structures and Optical Properties at Ambient RH

[23] The resulting humidograms with less hygroscopic (structure A); hygroscopic, nondeliquescent and without hysteresis (structure B); and hygroscopic, nondeliquescent and with hysteresis (structure C) curve structures, which characterized 99% of the measurements during the field campaign, are presented in Figure 5. Curve structures A, B and C existed during 12%, 76%, and 11% of the field campaign, respectively. A fourth curve structure (structure D), hygroscopic with deliquescence, was detected 1% of the time, but is excluded from further discussion because of its infrequent occurrence. The curve fit parameters and R^2 values describing f(RH, 26) for σ_{sp} and σ_{bsp} at all three wavelengths are provided in Figure 6 for curve structures A, B and C. Also included are averaged hygroscopic response factors, $f_{\sigma sp}$(82, 26), with R^2 values between the fitted and measured values ranging from 0.608 to 0.998.

[24] The average $f_{\sigma sp}$(82, 26) value for humidograms with less hygroscopic curve structure A was 1.38 ± 0.10 (Figure 5a). Aerosols that were hygroscopic with curve structures B and C had $f_{\sigma sp}$(82, 26) values of 1.98 ± 0.31 and 2.14 ± 0.40, respectively, with the major difference being the existence of hysteresis for curve structure C. These humidograms show the ambient aerosols' hydration state if the RH is decreased to 60% RH by comparing $f_{\sigma sp}$($60_{decrease}$, 26) values to $f_{\sigma sp}$(60, 26) values. The ARD between $f_{\sigma sp}$($60_{decrease}$, 26) values to $f_{\sigma sp}$(60, 26) was 3.4% when no hysteresis was observed (curve structures A and B). Such observations constitute 88% of the measurements during the field campaign. When hysteresis was observed during 12% of the field campaign (curve structures C and D), the ARD between $f_{\sigma sp}$($60_{decrease}$, 26) and $f_{\sigma sp}$(60, 26) for the lower branch of the hysteresis loop was 6.9%. An overall ARD of 3.8% indicates that the aerosol is unlikely to form metastable aerosol, even if the ambient RH decreased below the DRH of the submicrometer diameter aerosol during the field campaign.

[25] Values for σ_{sp}($RH_{ambient}$) and ω($RH_{ambient}$) were determined knowing the aerosols' hydration state (as described earlier), $f_{\sigma sp}$($RH_{ambient}$, 26) values, and the corresponding low RH σ_{sp} and σ_{ap} values. The regression equations for the three hygroscopic curve structures were used to calculate $f_{\sigma sp}$($RH_{ambient}$, 26) as 2.67 ± 0.84. The resulting values for σ_{sp}($RH_{ambient}$) and ω($RH_{ambient}$) were 110 ± 112 Mm^{-1} and 0.92 ± 0.06, respectively.

3.4. $f_{\sigma sp}$(RH, 26) and h(60) Values and Aerosol Chemical Properties

[26] Analysis of aerosol chemical composition provides insight into the dependence of the aerosol optical response to humidity and solute composition. For example, it was shown that $f_{\sigma sp}$(85, 40) decreased with increasing values of

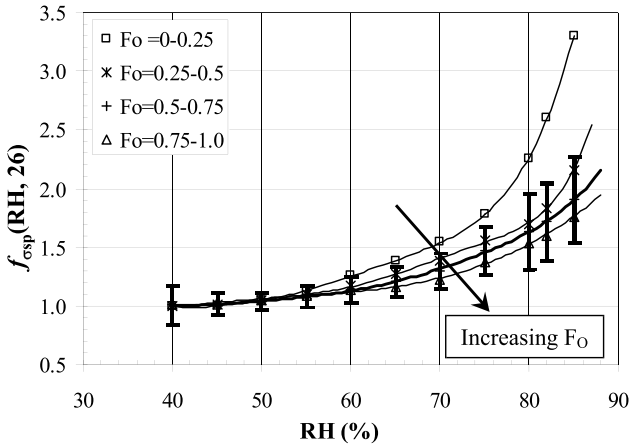

Figure 7. Humidograms measured at select F_O ($\frac{mass_{NR-POM}}{mass_{NR-POM}+mass_{NR-SO_4^{2-}}}$) values. Standard deviations for F_O = 0.5 − 0.75 are provided as vertical lines.

F_O and ER for three field campaigns [*Quinn et al.*, 2005]. In this study, the dependence of $f_{\sigma sp}$(RH, 26) on F_O and ER was studied for the RH range between 40% to 85% with increasing and decreasing RH conditions. The humidograms demonstrate that $f_{\sigma sp}$(82, 26) values decreased by 39% as F_O increased from 0–0.25 to 0.75–1.0 (Figure 7). The frequency of occurrence of the four F_O ranges (0–0.25, 0.25–0.5, 0.5–0.75, and 0.75–1.0) was 1.0%, 25.2%, 36.0% and 37.8%, respectively. The reduction in hygroscopic response with increasing F_O values was more evident at smaller rather than larger values of F_O. For example, $f_{\sigma sp}$(82, 26) was reduced by 29.6% when F_O increased from 0–0.25 to 0.25–0.5. However, $f_{\sigma sp}$(82, 26) was reduced by only 7.0% when F_O increased from 0.5–0.75 to 0.75–1.0. In contrast to the results describing the dependence of $f_{\sigma sp}$(82, 26) on F_O, there was no clear trend when describing the dependence of $f_{\sigma sp}$(82, 26) on ER (Figure 7). Such observation is consistent with the statistical analyses that describe single and multiple linear regressions for $f_{\sigma sp}$(82, 26) at the 0.95 confidence level as described below.

[27] Results from the single linear regressions for $f_{\sigma sp}$(82, 26) with F_O and $f_{\sigma sp}$(82, 26) with ER were both significant with their corresponding *p*-values <0.05 (Table 1). However, results from the multiple linear regression that considered $f_{\sigma sp}$(82, 26) with F_O and ER simultaneously indicate that F_O is significant (*p*-value <0.05), but ER (*p*-value > 0.05) is insignificant. The conclusive results for F_O, but the inconclusive results for ER are partially explained by their R^2 value of 0.53, which is influenced in part by the aerosols' mutual source regions, transport pathways, and transformation processes. These statistics indicate that $f_{\sigma sp}$(82, 26) decreases linearly with increasing F_O values, but there is no statistically significant dependence of $f_{\sigma sp}$(82, 26) on ER when considering the single and multiple regressions at the 0.95 confidence level.

[28] Results from the multiple linear regression that considered *h*(60) with F_O and ER simultaneously were statistically significant with both *p*-values < 0.05 (Table 1). However, results from the single linear regressions indicate that ER is significant (*p*-value < 0.05), but F_O is insignificant (*p*-value > 0.05). Therefore the dependence of *h*(60) on ER is conclusive, but not for F_O. The conclusive results for ER, but the inconclusive results for F_O are partially explained once again by their R^2 value as mentioned earlier. These statistics indicate that *h*(60) increases linearly with increasing values of ER, but there is no statistically significant dependence of *h*(60) on F_O when considering the single and multiple regressions at the 0.95 confidence level. Overall, the statistical analyses for $f_{\sigma sp}$(82, 26) and *h*(60) indicate that (1) a larger POM mass fraction results in a less hygroscopic aerosol based on its optical properties and (2) a reduction in acidity (larger ER values) allows for more of the aerosol to potentially exist in a metastable state at RH = 60%.

[29] A series of hourly humidograms obtained during DOY 212 (30 July 2004) illustrate the temporal evolution of the aerosol's hygroscopic properties in addition to its F_O and ER values (Figure 8). On that day, the ship passed through an urban plume that came from the west, to Boston, and then veered north to the ship [*Quinn et al.*, 2006]. Starting from Figure 8a and moving in the clockwise direction, the ambient aerosol initially displayed a hygroscopic but monotonic curve (curve structure B) with F_O = 0.70 and ER = 0.54. The following humidograms demonstrated the development and then a dissipation of hysteresis between the lower and upper branches of the humidograms (curve structure C) as ER values increased by 63% to 0.88 and then returned to 0.54. However, F_O values decreased by only 21% to 0.55 and then increased back to 0.69 resulting in an almost constant value for $f_{\sigma sp}$(82, 26) of 2.0 ± 0.1. Such response in $f_{\sigma sp}$(82, 26) is consistent with an almost constant calculated $f_{\sigma sp}$(82, 26) value of 1.97 ± 0.04 that was determined with the multiple linear regression for $f_{\sigma sp}$(82, 26) as described above.

Table 1. Regression Analysis Results for Optical Properties Against Two Chemical Parameters

	Multiple Linear Regression		Singular Linear Regression	
	Estimate[c]	*p*-Value	Estimate[a]	*p*-Value
		$f\sigma_{sp}$(82, 26)		
F_O[b]	−0.60	5.15E-07	−0.69	5.17E-15
ER[c]	−0.11	0.229	−0.43	9.81E-10
		h(60)		
F_O	−0.05	0.0223	0.02	0.198
ER	0.09	2.16E-07	0.07	1.33E-06

[a]Estimate = regression coefficient, β_i.
[b]F_O = mass fraction of particulate organic matter (POM, $F_O = \frac{mass_{NR-POM}}{mass_{NR-POM}+mass_{NR-SO_4^{2-}}}$).
[c]ER = molar equivalence ratio = $\frac{mole_{NH_4^+}}{mole_{NO_3^-}+2\,mole_{SO_4^{2-}}}$.

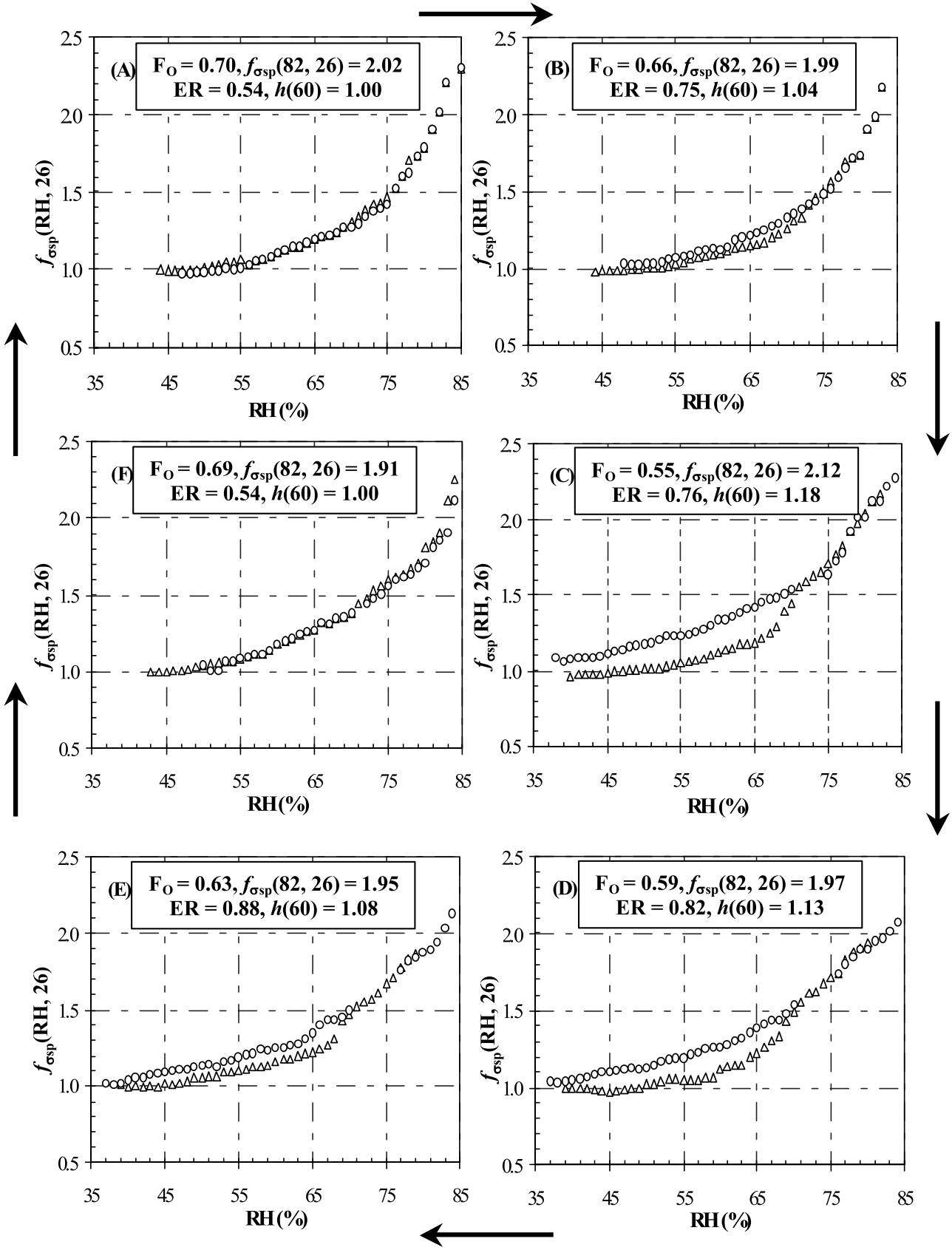

Figure 8. Temporal variation of hourly humidograms with changing chemistry. (a–e) Six humidograms presented chronographically, with Figure 8a being the earliest.

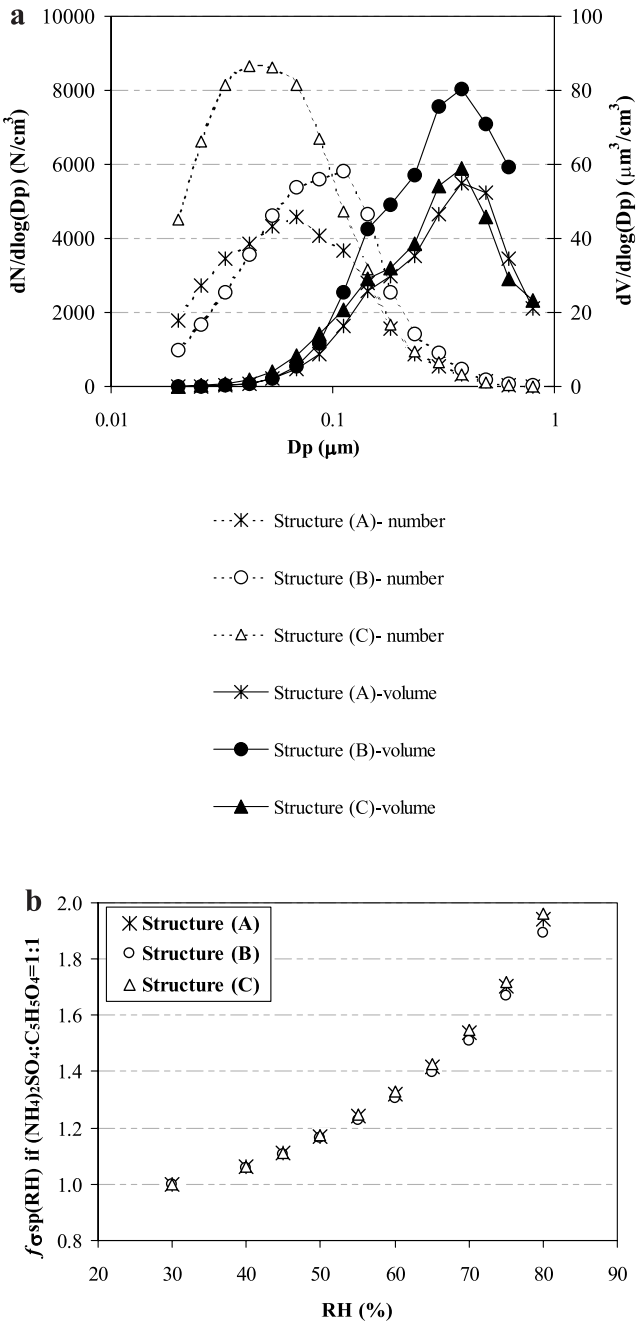

Figure 9. (a) Particle number- and volume-size distributions measured at RH = 60%. (b) Modeled humidogram curve structures for size distributions shown in Figure 9a, assuming that the aerosol consisted of $(NH_4)_2SO_4$ and glutaric acid at 1:1 mass ratio.

[30] An aerosol's initial dry particle size distribution can also influence its change in optical properties with a change in ambient or instrumental RH [*Hegg et al.*, 1993]. Therefore particle size distributions measured by the DMPS were averaged over each of the same time periods when the three humidogram curve structures (Figure 5) were observed. This was done to evaluate whether dry particle size distributions (number- and volume-size distributions shown in Figure 9a) had an influence on humidogram curve structure. These three size distributions correspond to humidogram curve structures (A, Figure 5a) with F_O = 0.87 ± 0.04, (B, Figure 5b) with F_O = 0.62 ± 0.19, and (C, Figure 5c) with F_O = 0.29 ± 0.16. Within the "optically effective" diameter range of 0.1 μm and larger, the volume-size distributions, which are most closely related to the light scattering distributions, showed less difference among the three cases when compared to the number-size distributions. The mean diameters and geometric standard deviations of the volume distributions were almost identical. This indicates that the aerosols' size distributions during the field campaign were stable and are not expected to cause the observed difference in humidogram curve structures. This was verified by modeling the aerosols' particle size dependence on RH [*Svenningsson et al.*, 2005; *Prenni et al.*, 2003; *Choi and Chan*, 2002; *Peng et al.*, 2001; *Tang*, 1996] and their light scattering properties as a function of RH with Mie scattering code [*Bohren and Huffman*, 1983] using these size distributions. These particles were assumed to be internally mixed with $(NH_4)_2SO_4$ and glutaric acid. Glutaric acid was used as a surrogate organic compound because data were not available to describe the composition of the organic material in the ambient particles, and dicarboxylic acids represent a major component of the water-soluble primary and secondary particulate organic carbon mass in the atmosphere [*Sempere and Kawamura*, 1994; *Saxena and Hildemann*, 1996]. Hygroscopic growth factors in d_p, calculated on the basis of the Zdanovskii-Stokes-Robinson (ZSR) method [*Choi and Chan*, 2002], were used to convert the measured particle size distributions at 60% RH to distributions at 30% RH. Humidograms were then modeled for an internal mixture of $(NH_4)_2SO_4$ and glutaric acid at F_O values of 0.75, 0.5, and 0.25 for all three curve structures (Figure 5) to describe $f_{\sigma sp}$(RH, 26) with RH values ranging between 30% and 82%. $f_{\sigma sp}$(82, 26) values for all nine of these test cases range from 1.86 to 1.96. Results for F_O = 0.5 and curve structures A, B, and C (Figure 5) are presented in Figure 9b with $f_{\sigma sp}$(82, 26) values ranging from 1.90 to 1.96 to demonstrate the similarity of the resulting $f_{\sigma sp}$(RH, 26) values. The calculated $f_{\sigma sp}$(82, 26) values compare favorably to the measured $f_{\sigma sp}$(82, 26) value of 1.98 ± 0.31 for the humidogram curve that exists 76% of the sampling period (Figure 5b). The calculated $f_{\sigma sp}$(RH, 26) values described in Figure 9b differ by <3.5% ARD. Thus the small variability of the size distributions within the range observed in NEAQS-ITCT 2004 had little effect on the variability of the measured $f_{\sigma sp}$(RH, 26) values. By extension, the variability in $f_{\sigma sp}$(RH, 26) measured by the humidograph during the field campaign implies that this was largely due to variability in chemical composition.

3.5. Case Studies for Select Source Regions

[31] Several aerosol source regions were identified during the field campaign, including local emissions from urban regions, regional emissions from the northeast U.S. urban corridor (Washington, D. C., New York, and Boston), and distant emissions from Midwest industrial regions and North American forest fires [*Quinn et al.*, 2006]. The periods when aerosol was received from these source regions are indicated by colored bars along the top of the Figure 4. Averages and standard deviations of σ_{sp}, ω, $\mathring{a}$, b,

Table 2. Aerosol Composition[a] and Optical Properties for Case Studies

Source	ER[a,b]	F_O[a,c]	σ_{sp}, Mm^{-1}	ω	å	b	$f_{\sigma sp}(82, 26)$
			Local Source Regions				
Boston Harbor	1.1 ± 0.55	0.91 ± 0.05	13.9 ± 2.3	0.77 ± 0.12	1.87 ± 0.12	0.15 ± 0.01	1.52 ± 0.14
			Regional Source Regions				
NE U.S. plume 30 Jul	0.83 ± 0.19	0.69 ± 0.06	86.9 ± 13.5	0.92 ± 0.02	1.27 ± 0.07	0.11 ± 0.01	1.83 ±0 .08
NE U.S. plume 11–12 Aug	0.57 ± 0.13	0.36 ± 0.03	65.0 ± 16.7	0.97 ± 0.01	2.07 ± 0.07	0.12 ± 0.01	2.12 ± 0.18
			Distant Source Regions				
East Gulf of Maine 9 Jul	0.22 ± 0.06	0.28 ± 0.03	18.0 ± 11.4	0.92 ± 0.04	1.80 ± 0.10	0.13 ± 0.02	1.92 ± 0.39
East Gulf of Maine 19 Jul	0.15 ± 0.06	0.30 ± 0.02	10.6 ± 10.9	0.92 ± 0.07	1.55 ± 0.41	0.16 ± 0.08	1.75 ± 0.21
Forest fires 14 Jul	0.93 ± 0.42	0.86 ± 0.04	32.6 ± 30.1	0.96 ± 0.01	1.12 ± 0.09	0.08 ± 0.05	1.40 ± 0.13

[a]Aerosol composition data cited from *Quinn et al.* [2006].

[b]ER = molar equivalence ratio = $\frac{mole_{NH_4^+}}{mole_{NO_3^-} + 2\ mole_{SO_4^{2-}}}$.

[c]F_O = mass fraction of particulate organic matter (POM, $F_O = \frac{mass_{NR-POM}}{mass_{NR-POM} + mass_{NR-SO_4^{2-}}}$).

$f_{\sigma sp}(82, 26)$ and $h(60)$ for the local, regional and distant source regions are shown in Table 2. These case studies were identified to further evaluate the influence of aerosol composition (F_O and ER) on the aerosols' optical properties (σ_{sp}, ω, å, b, and $f_{\sigma sp}(82, 26)$). Each of these case studies included 7 to 21 out of 529 ambient humidograms. For the Boston Harbor case, where measurements occurred near the source region, *Quinn et al.* [2006] observed that ER was near one (1.10 ± 0.55) with a large mass fraction of POM (F_O = 0.91 ± 0.05). Boston Harbor aerosol exhibited a relatively low $f_{\sigma sp}(82, 26)$ (1.52 ± 0.14), σ_{sp} (13.9 ± 2.3), and ω (0.77 ± 0.12) values, and high b (0.15 ± 0.01) values. As the distance from the source region increased (e.g., northeastern U. S. plume, 11–12 August), the aerosol became more acidic (ER = 0.57 ± 0.13) with a lower mass fraction of POM (F_O = 0.36 ± 0.03) and had higher $f_{\sigma sp}(82, 26)$ (2.12 ± 0.18), σ_{sp} (65.0 ± 16.7), and ω (0.97 ± 0.01) values, and lower b (0.12 ± 0.01) values. Comparison of $f_{\sigma sp}(82, 26)$ values for these two cases indicates that the aerosol is less hygroscopic when the aerosol has a larger mass fraction of POM with a larger ER value. The dependence of $f_{\sigma sp}(RH, 26)$ on F_O is also graphically presented as averaged humidograms to describe four of the case studies in Figure 10. The same trend of decreasing $f_{\sigma sp}(82, 26)$ values with increasing F_O values is observed for the case studies (Figure 10) as for the entire field campaign (Figure 7).

[32] An interesting comparison is observed when examining the Boston Harbor and Forest Fire cases. The Boston Harbor is a fresh, polluted aerosol featuring a smaller mean diameter (as seen with the larger b and å values) and higher light-absorbing content (as seen with the lower value of ω). In contrast, the aged forest fire aerosol is much larger in mean size (as seen from lower b and å values) and nearly a pure scattering aerosol. Nonetheless, the hygroscopic growth properties are very similar in structure and magnitude with $f_{\sigma sp}(82, 26)$ of 1.52 and 1.40 for these two cases (Table 2 and Figure 10). This result underscores the importance of F_O values greater than 0.8 in both cases, in influencing hygroscopic growth properties despite the differing source regions of the aerosol.

[33] The intensive aerosol parameters, ω, b, å, $f_{\sigma sp}(82, 26)$, and $h(60)$, for the local, regional and distant case studies are compared to average values from the ACE-Asia, ACE-2, ACE-1 field campaigns and Bondville Environmental Aerosol Research Site (BEARS) measurements (Table 3). The emission types for the local, regional or distant case studies do not specifically match the source types for the previous field studies, although values obtained for the optical parameters during NEAQS-ITCT 2004 are within the range of values reported in Table 3.

3.6. RH and Wavelength Dependence of Aerosol's Optical Properties

[34] Values of ω changed by 4% from 0.92 at RH = 26% to 0.96 at RH = 82%. Values of å and b decreased linearly as RH increased from 40% to 85% (Figure 11). Aerosol particle size increased when taking up water with increasing RH values, which resulted in more total light scattering relative to light absorption, more forward scattering relative to backscattering, but less sensitivity of total light scattering to changes in visible λ values. Therefore smaller values of b and å are expected with increasing RH values [*Bohren and Huffman*, 1983]. The RH dependence of b has important implications to radiative forcing as knowledge of b permits the estimation of the asymmetry parameter used in radiative transfer calculations [*Bates et al.*, 2006].

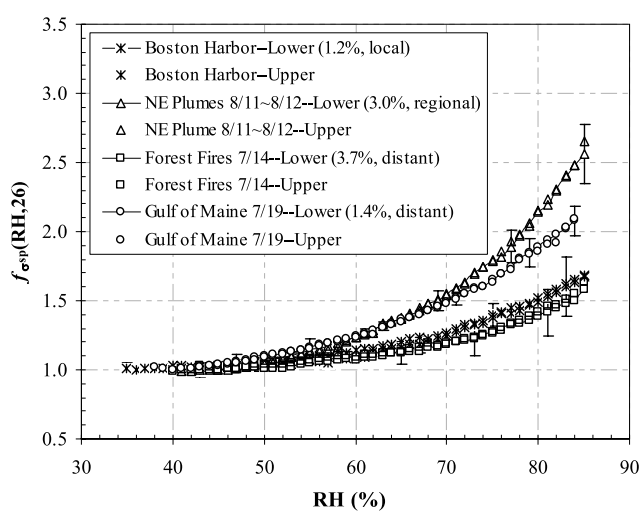

Figure 10. Humidograms for select case studies representative of different source regions. The frequency of occurrence and source category are marked in parentheses. Standard deviations are provided as vertical lines.

Table 3. Optical Properties of Submicrometer Diameter Ambient Aerosols ($d_p \leq 1$ μm) Measured During Select Field Campaigns

Air Mass	σ_{sp}[a]	ω[b]	$\mathring{a}$[c]	b	$f_{\sigma sp}(82, 26)$	$h(60)$
			NEAQS-ITCT, 2004			
Local	36.2 ± 25.7	0.91 ± 0.08	2.00 ± 0.13	0.14 ± 0.02	2.06 ± 0.19	1.00 ± 0.05
Regional	55.0 ± 37.5	0.92 ± 0.02	1.61 ± 0.34	0.12 ± 0.02	1.84 ± 0.11	1.04 ± 0.09
Distant	29.0 ± 18.8	0.93 ± 0.04	1.53 ± 0.33	0.12 ± 0.02	1.53 ± 0.31	1.00 ± 0.07
			ACE-Asia, 2001[d]			
Marine	7.1 ± 2.8	0.97 ± 0.02	1.30 ± 0.75	NA[e]	2.95 ± 0.39	1.6
Polluted	41 ± 24	0.92 ± 0.03	1.72 ± 0.31	0.09 ± 0.02	2.52 ± 0.27	1.3
Volcanic	94 ± 61	0.95 ± 0.06	1.68 ± 0.37	0.07 ± 0.02	2.61 ± 0.17	1.0
Dust	82 ± 33	0.91 ± 0.04	1.39 ± 0.34	0.11 ± 0.03	2.10 ± 0.29	1.25
			ACE-2, 1997[f]			
Polluted	42.8 ± 19.1	0.93 ± 0.05	2.47 ± 0.13	0.12 ± 0.02	1.48 ± 0.10	NA
Clean	6.5 ± 4.8	0.94 ± 0.03	2.57 ± 0.38	0.15 ± 0.03	1.86 ± 0.24	NA
			ACE-1, 1995[g]			
Clean marine	3.6 ± 2.0	$\geq$ 0.986[h]	1.06 ± 0.61	0.12 ± 0.03	2.46 ± 0.20	NA
Non-clean-marine	5.4 ± 3.0	$\geq$0.986[h]	1.38 ± 0.52	0.13 ± 0.02	2.36 ± 0.40	NA
			BEARS, 1996–2000[i]			
Continental	42	0.91	2.1	0.13	NA	NA

[a]Unless otherwise specified, all results presented here are for RH < 30% and λ = 550 nm except for ACE-Asia where ω, $\mathring{a}$, and b values are for ambient conditions.
[b]ω values for ACE-2 referred to aerosol particles with $d_p \leq 10$ μm.
[c]$\mathring{a}$ values are calculated for λs of 450 nm and 550 nm except for ACE-2 and ACE-1, where λs of 550 nm and 700 nm were used.
[d]*Carrico et al.* [2003].
[e]NA, not available.
[f]*Carrico et al.* [2000].
[g]*Carrico et al.* [2000].
[h]*Quinn and Coffman* [1998].

[35] The wavelength dependences of $\mathring{a}$, b and $f_{\sigma sp}(82, 26)$ were also investigated. The dependency of $\mathring{a}$ on λ was larger at longer visible wavelengths when compared to shorter visible wavelengths: $\mathring{a}(450, 550) < \mathring{a}(450, 700) < \mathring{a}(550, 700)$, however $\mathring{a}(450, 700)$ is within 8% of $\mathring{a}(450, 550)$ and $\mathring{a}(550, 700)$. Values for b increased with increasing values of λ indicating that backscattering by the aerosol increases more than forward scattering as λ increases over the measured wavelengths. Values for $f_{\sigma sp}(82, 26)$ also increased with λ, however $f_{\sigma sp}(82, 26)$ values at 550 nm were within 9% of those measured at 450 nm and 700 nm. The relatively insensitive responses of $\mathring{a}$ and $f_{\sigma sp}(82, 26)$ to λ indicate that $\mathring{a}$ values at 450 nm and 700 nm, and $f_{\sigma sp}(82, 26)$ values at 550 nm are within 8% and 9% of their values at λs of 450 nm and 700 nm, respectively.

3.7. Sensitivity of Aerosol Radiative Forcing to Variations in Aerosol Optical Parameters

[36] The sensitivity of top of the atmosphere (TOA) aerosol radiative forcing to changes in b, ω, and σ_{sp} with RH were estimated from the *Haywood and Shine* [1995] equation. The calculations are not intended to provide an accurate estimate of TOA forcing but rather a sensitivity study. The common assumptions made for the calculations are: the daylight fraction is equal to 0.5, fraction of cloud cover is equal to 0.6, and surface albedo is equal to 0.07, the top of the atmosphere radiative flux is 1,370 W m^{-2}, the transmittance of light through the atmosphere above the aerosol layer is 0.76, and there is no geographical variation or zenith angle dependence of the parameters used in the equation. In addition, the Henyey-Greenstein phase function was used to calculate the upscatter fraction, $\overline{\beta}$, from b [*Wiscombe and Grams*, 1976; *Sheridan and Ogren*, 1999; *Quinn and Bates*, 2005].

[37] The sensitivity of TOA aerosol radiative forcing to changes in RH was determined by using the values of b, ω, and $f_{\sigma sp}(\mathrm{RH}, 26)$ at $\mathrm{RH}_{ambient}$ = 26% and $\mathrm{RH}_{ambient}$ = 82% as determined by the hourly humidograms that were obtained during the entire field campaign. Values for σ_{sp} at $\mathrm{RH}_{ambient}$ = 26% and $\mathrm{RH}_{ambient}$ = 82% were then determined with σ_{sp} values at 26% RH that were then multiplied by $f_{\sigma sp}(26, 26)$ (which is one) and $f_{\sigma sp}(\mathrm{RH}_{ambient} = 82, 26)$, respectively.

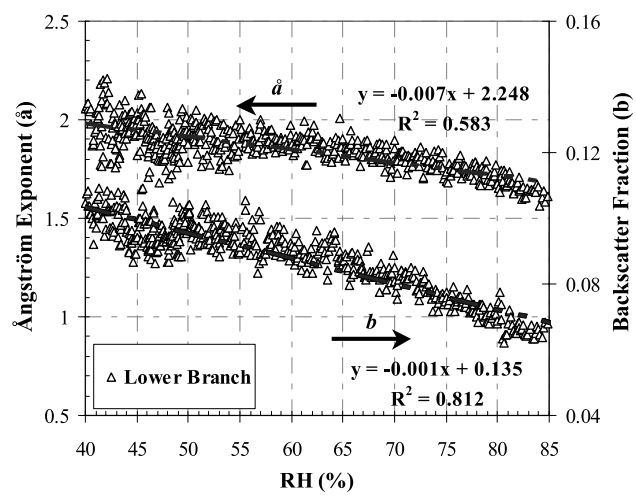

Figure 11. RH dependence of $\mathring{a}$ for λ = 450 and 550 nm and b at λ = 550 nm. Regressions are provided for the lower branches of the hysteresis loop.

Values for σ_{ap} used for the calculations were as measured during each of the humidograms, and assumed to be independent of RH. The height of the well-mixed aerosol layer was assumed to be 500 m while calculating the aerosol optical depth (AOD). The TOA aerosol forcing changed from -0.86 W m^{-2} (AOD = 0.03) at RH = 26% to -1.34 W m^{-2} (AOD = 0.05) at RH = 82%, or a 57% increase in cooling when considering aerosol forcing at high to low RH conditions. However, if b, ω, and σ_{sp} were each allowed to change while increasing RH from 26% to 82% but keeping the other two optical properties as measured at 26% RH, then TOA aerosol radiative forcing would decrease by 16%, increase by 3%, and increase by 79%, respectively.

4. Summary and Conclusions

[38] Marine boundary layer aerosol particles were sampled aboard the NOAA R/V *Ronald H. Brown* during the NEAQS-ITCT field campaign from DOY 187–226 (5 July through 13 August 2004). A scanning-relative humidity (RH) nephelometry system (humidograph) quantified light scattering by submicrometer diameter aerosol particles ($d_p \leq 1$ μm) as a function of increasing and decreasing RH conditions ($f_{\sigma sp}$(RH, RH$_{ref}$), where RH$_{ref}$ = low reference RH value), direction of light scattered (total (σ_{sp}) and back (σ_{bsp})), and wavelength of light (λ) at 450 nm, 550 nm, and 700 nm during transits along the northeast coast of North America. These results were integrated with additional light scattering, light absorption, particle size, and composition measurements that occurred on the ship during the field campaign. Extensive and intensive aerosol parameters were quantified at RH$_{ref}$ (26 ± 4% RH) over the entire sampling period: σ_{sp} = 42.9 ± 35.2 Mm^{-1}; b = 0.12 ± 0.02; and ω = 0.92 ± 0.06 for λ = 550 nm; and $\mathring{a}$ = 2.1 ± 0.3 for λ = 450 and 550 nm.

[39] Humidogram curve structure during the entire field campaign is summarized by four curve structures: structure A, less hygroscopic (12% frequency); structure B, hygroscopic, nondeliquescent without hysteresis (76% frequency); structure C, hygroscopic, nondeliquescent with hysteresis (11% frequency); and structure D, hygroscopic and deliquescent (1% frequency). Values of ω increased by 4% from 0.92 at RH = 26% to 0.96 at RH = 82% while values of $\mathring{a}$ and b decreased linearly with increasing RH. The sensitivity of top of the atmosphere (TOA) aerosol radiative forcing to changes in ω, b, and σ_{sp} with RH showed a 57% increase in cooling when considering aerosol forcing at RH = 82% to RH = 26% depending on the assumptions used with the calculations. Values for $\mathring{a}(\lambda_1, \lambda_2)$, b, and $f_{\sigma sp}$(82, 26) increased with increasing values of λ. However, values for $\mathring{a}(\lambda_1, \lambda_2)$ at 450 nm and 700 nm and values for $f_{\sigma sp}$(82, 26) at 550 nm were observed within 8% and 9% of the measurements at wavelengths within 450 nm and 700 nm. The dependence of $f_{\sigma sp}$(RH, 26) on mass fraction of particulate organic matter (POM, $F_O = \frac{mass_{NR-POM}}{mass_{NR-POM} + mass_{NR-SO_4^{2-}}}$) and the molar equivalence ratio (ER $= \frac{mole_{NH_4^+}}{mole_{NO_3^-} + 2\ mole_{SO_4^{2-}}}$) was analyzed as RH was scanned between 40% RH and 85% RH. The aerosol's optical hygroscopicity, represented as $f_{\sigma sp}$(RH, 26), was observed to decrease with increasing F_O values. Multiple and single linear regression analyses for $f_{\sigma sp}$(82, 26) and h(60) against F_O and ER values were completed to evaluate the significance of these two chemical parameters in influencing the aerosol's optical properties at a 0.95 confidence level. Increasing F_O values resulted in less hygroscopic aerosol (lower values of $f_{\sigma sp}$(82, 26)) and increasing ER values resulted in an increase in the ability of the aerosol to exhibit hysteresis, when considering statistically significant results from multiple and single linear regressions.

[40] Case studies with local, regional and distant source regions were used to further evaluate the influence of aerosol composition (F_O and ER) on optical properties. In general, the aerosol was less hygroscopic (lower values of $f_{\sigma sp}$(82, 26)) with increasing F_O and ER values.

[41] The optical data summarized here for the marine boundary layer along the northeast coast of North America can be used to refine and constrain radiative transfer models and thus reduce the uncertainties in the modeled aerosol radiative forcing of climate.

Notation

Acronyms	
AMS	aerosol mass spectrometer.
AOD	aerosol optical depth.
ARD	absolute relative difference.
BEARS	Bondville Environmental Aerosol Research Site.
CCN	cloud condensation nuclei.
CRH	crystallization relative humidity.
CTM	chemical transport model.
RTM	radiative transfer model.
DMPS	differential mobility particle sizer.
DRH	deliquescence relative humidity.
ER	equivalence ratio.
NOAA-PMEL	National Oceanic and Atmospheric Administration–Pacific Marine Environment Laboratory
NR	nonrefractory.
POM	particulate organic matter.
PSAP	particle soot absorption photometer.
RH	relative humidity.
RR	Radiance Research.
STP	standard temperature and pressure.
TOA	top of atmosphere.
ZSR	Zdanovski-Stokes-Robinson.
Parameter notation	
σ_{sp}	total light scattering coefficient.
σ_{bsp}	backscattering coefficient.
λ	wavelength.
ω	single scattering albedo.
$\mathring{a}$	Ångström exponent.
b	hemispheric backscatter fraction.
F_O	mass fraction of POM.
ER	acidity (as described by the molar equivalence ratio with respect to ammonium, nitrate, and sulfate).
$f_{\sigma sp}$(RH, RH$_{Ref}$)	dependence of the aerosol's σ_{sp} values with changes in RH.
T	temperature.
σ_{ep}	light extinction coefficient.
σ_{ap}	light absorption coefficient.
h(RH)	hysteresis factor.
RH$_{Ref}$	reference RH.

d_p particle diameter.
β_i linear regression coefficient.
p-value probability of wrongly rejecting the null hypothesis if in fact true.

[42] **Acknowledgments.** We thank the officers and crew of NOAA R/V *Ronald H. Brown* for their cooperation and D. Coffman, D. Hamilton, and J. Johnson for technical support. We also thank Adam Martinsek for his discussions about the statistical analyses that strengthened the results and discussions. This research was funded by the Atmospheric Constituents Project of the NOAA Climate and Global Change Program, the NOAA Office of Oceanic and Atmospheric Research, the NOAA Health of the Atmosphere Program, and the New England Air Quality Study.

References

Albrecht, B. A. (1989), Aerosols, cloud microphysics, and fractional cloudiness, *Science*, *245*, 1227–1230.

Ångström, A. (1964), Parameters of atmospheric turbidity, *Tellus*, *16*, 64–75.

Anderson, T. L., and J. A. Ogren (1998), Determining aerosol radiative properties using the TSI 3563 Integrating Nephelometer, *Aerosol Sci. Technol.*, *29*, 57–69.

Anderson, T. L., R. J. Charlson, S. E. Schwartz, R. Knutti, O. Boucher, H. Rodhe, and J. Heintzenberg (2003), Climate forcing by aerosols—A hazy picture, *Science*, *300*(5622), 1103–1104.

Bates, T. S., B. J. Huebert, J. L. Gras, F. B. Griffiths, and P. A. Durkee (1998), International Global Atmospheric Chemistry (IGAC) Project's First Aerosol Characterization Experiment (ACE 1): Overview, *J. Geophys. Res.*, *103*(D13), 16,297–16,318.

Bates, T. S., D. J. Coffman, D. S. Covert, and P. K. Quinn (2002), Regional marine boundary layer aerosol size distributions in the Indian, Atlantic, and Pacific Oceans: A comparison of INDOEX measurements with ACE-1, ACE-2, and Aerosols99, *J. Geophys. Res.*, *107*(D19), 8026, doi:10.1029/2001JD001174.

Bates, T. S., P. K. Quinn, D. J. Coffman, J. E. Johnson, and A. M. Middlebrook (2005), Dominance of organic aerosols in the marine boundary layer over the Gulf of Maine during NEAQS 2002 and their role in aerosol light scattering, *J. Geophys. Res.*, *110*, D18202, doi:10.1029/2005JD005797.

Bates, T. S., et al. (2006), Aerosol direct radiative effects over the northwest Atlantic, northwest Pacific, and North Indian oceans: Estimates based on in-situ chemical and optical measurements and chemical transport modeling, *Atmos. Chem. Phys.*, *6*, 1657–1732, SRef-ID:1680-7324/acp/2006-6-1657.

Bellouin, N., O. Boucher, J. Haywood, and M. S. Reddy (2005), Global estimate of aerosol direct radiative forcing from satellite measurements, *Nature*, *438*(7071), 1138–1141.

Bohren, C. F., and D. R. Huffman (1983), *Absorption and Scattering of Light by Small Particles*, 530 pp., John Wiley, Hoboken, N. J.

Bond, T. C., T. L. Anderson, and D. Campbell (1999), Calibration and intercomparison of filter based measurements of visible light absorption by aerosols, *Aerosol Sci. Technol.*, *30*, 582–600.

Boucher, O., and T. L. Anderson (1995), General circulation model assessment of the sensitivity of direct climate forcing by anthropogenic sulfate aerosols to aerosol size and chemistry, *J. Geophys. Res.*, *100*(D12), 26,117–26,134.

Carrico, C. M., M. J. Rood, and J. A. Ogren (1998), Aerosol light scattering properties at Cape Grim, Tasmania, during the First Aerosol Characterization Experiment (ACE 1), *J. Geophy. Res.*, *103*(D13), 16,565–16,574.

Carrico, C. M., M. J. Rood, J. A. Ogren, C. Neusüß, A. Wiedensohler, and J. Heintzenberg (2000), Aerosol optical properties at Sagres, Portugal, during ACE 2, *Tellus, Ser. B*, *52*, 694–716.

Carrico, C. M., P. Kus, M. J. Rood, P. K. Quinn, and T. S. Bates (2003), Mixtures of pollution, dust, sea salt and volcanic aerosol during ACE-Asia: Aerosol radiative properties as a function of relative humidity, *J. Geophys. Res.*, *108*(D23), 8650, doi:10.1029/2003JD003405.

Carrico, C. M., S. M. Kreidenweis, J. L. Collett Jr., and W. C. Malm (2005), Hygroscopic growth behavior of a carbon dominated aerosol in Yosemite National Park, *Atmos. Environ.*, *39*(8), 1393–1404.

Charlson, R. J., A. Vanderpol, D. S. Covert, A. P. Waggoner, and N. C. Ahlquist (1974), Sulfuric acid-ammonium sulfate aerosol: Optical detection in the St. Louis region, *Science*, *184*, 156–158.

Charlson, R. J., J. Langner, H. Rodhe, C. B. Leovy, and S. G. Warren (1991), Perturbation of the Northern Hemisphere radiative balance by backscattering from anthropogenic sulfate aerosols, *Tellus, Ser. A*, *43*(4), 152–163.

Charlson, R. J., S. E. Schwartz, J. M. Hales, R. D. Cess, J. A. Coakley Jr., J. E. Hansen, and D. J. Hofmann (1992), Climate forcing by anthropogenic aerosols, *Science*, *255*, 423–430.

Chin, M., A. Chu, R. Levy, L. Remer, Y. Kaufman, B. Holben, T. Eck, P. Ginoux, and Q. Gao (2004), Aerosol distribution in the Northern Hemisphere during ACE-Asia: Results from global model, satellite observations, and Sun photometer measurements, *J. Geophys. Res.*, *109*, D23S90, doi:10.1029/2004JD004829.

Choi, M. Y., and C. K. Chan (2002), The effects of organic species on the hygroscopic behaviors of inorganic aerosols, *Environ. Sci. Technol.*, *36*, 2422–2428.

Covert, D. S., R. J. Charlson, and N. C. Ahlquist (1972), A study of the relationship of chemical composition and humidity to light scattering by aerosols, *J. Appl. Meteorol.*, *11*(6), 968–976.

Fox, J. (1997), *Applied Regression Analysis, Linear Models, and Related Methods*, chap. 5, pp. 85–110, Sage Publ. Inc, Thousand Oaks, Calif.

Hansson, H. C., M. J. Rood, S. Koloutsou-Vakakis, K. Hämeri, D. Orsini, and A. Wiedensohler (1998), NaCl aerosol particle hygroscopicity dependence on mixing with organic compounds, *J. Atmos. Chem.*, *31*, 321–346.

Haywood, J. M., and K. P. Shine (1995), The effect of anthropogenic sulfate and soot aerosol on the clear sky planetary radiation budget, *Geophys. Res. Lett.*, *22*, 603–606.

Hegg, D., T. Larson, and P. F. Yuen (1993), Theoretical study of the effect of relative humidity on light scattering by tropospheric aerosols, *J. Geophys. Res.*, *98*(D10), 18,435–18,439.

Heintzenberg, J., R. J. Charlson, A. D. Clarke, C. Liousse, V. Ramaswamy, K. P. Shine, M. Wendisch, and G. Helas (1997), Measurements and modeling of aerosol single-scattering albedo: Progress, problems, and prospects, *Contrib. Atmos. Phys.*, *70*(4), 249–263.

Houghton, J. T., Y. Ding, D. J. Griggs, M. Noguer, P. J. van der Linden, X. Dai, and K. Maskell (Eds.) (2001), *Climate Change 2001: The Scientific Basis—Contribution of Working Group I to the Third Assessment Report of the Intergovernmental Panel on Climate Change*, 892 pp., Cambridge Univ. Press, New York.

Huebert, B. J., T. Bates, P. B. Russell, G. Shi, Y. J. Kim, K. Kawamura, G. Carmichael, and T. Nakajima (2003), An overview of ACE-Asia: Strategies for quantifying the relationships between Asian aerosols and their climatic impacts, *J. Geophys. Res.*, *108*(D23), 8633, doi:10.1029/2003JD003550.

Kiehl, J. T., T. L. Schneider, P. J. Rasch, M. C. Barth, and J. Wong (2000), Radiative forcing due to sulfate aerosols from simulations with the National Center for Atmospheric Research Community Climate Model, Version 3, *J. Geophys. Res.*, *105*(D1), 1441–1457.

Koloutsou-Vakakis, S., C. M. Carrico, P. Kus, M. J. Rood, Z. Li, R. Shrestha, J. A. Ogren, J. Chow, and J. G. Watson (2001), Aerosol properties at a mid-latitude Northern Hemisphere continental site, *J. Geophys. Res.*, *106*(D3), 3019–3032.

Kus, P. (2003), Physical and chemical properties of laboratory and ambient aerosols related to climate change, Ph.D. Dissertation, Univ. of Ill. At Urbana-Champaign, Urbana.

Kus, P., C. M. Carrico, M. J. Rood, and A. Williams (2004), Measured and modeled light scattering values for dry and hydrated laboratory aerosols, *J. Atmos. Oceanic Technol.*, *21*(7), 981–994.

Larson, T. V., N. C. Ahlquist, R. E. Weiss, D. S. Covert, and A. P. Waggoner (1982), Chemical speciation of H_2SO_4/ $(NH_4)_2SO_4$ particles using temperature and relative humidity controlled nephelometry, *Atmos. Environ.*, *16*, 1587–1590.

Lohmann, U., and J. Feichter (2005), Global indirect aerosol effects: A review, *Atmos. Chem. Phys.*, *5*, 715–737.

Malm, W. C., D. E. Day, C. Carrico, S. M. Kreidenweis, J. L. Collett Jr., G. McMeeking, T. Lee, J. Carrillo, and B. Schichtel (2005), Intercomparison and closure calculations using measurements of aerosol species and optical properties during the Yosemite Aerosol Characterization Study, *J. Geophys. Res.*, *110*, D14302, doi:10.1029/2004JD005494.

Marshall, S. F., D. S. Covert, and R. J. Charlson (1995), Relationship between asymmetry factor and backscatter ratio: Implications for aerosol climate forcing, *Appl. Opt.*, *34*, 6306–6311.

Peng, C., M. N. Chan, and C. K. Chan (2001), The hygroscopic properties of dicarboxylic and multifunctional acids: Measurements and UNIFAC predictions, *Environ. Sci. Technol.*, *35*(22), 4495–4501.

Pilat, M. J., and R. J. Charlson (1966), Theoretical and optical studies of humidity effects on the size distribution of hygroscopic aerosol, *J. Rech. Atmos.*, *1*, 165–170.

Prenni, A. J., P. J. De Mott, and S. M. Kreidenweis (2003), Water uptake of internally mixed particles containing ammonium sulfate and dicarboxylic acids, *Atmos. Environ.*, *37*(30), 4243–4251.

Quinn, P. K., and T. S. Bates (2005), Regional aerosol properties: Comparisons of boundary layer measurements from ACE 1, ACE 2, Aerosols99, INDOEX, ACE Asia, TARFOX, and NEAQS, *J. Geophys. Res.*, *110*, D14202, doi:10.1029/2004JD004755.

Quinn, P. K., and D. J. Coffman (1998), Local closure during the First Aerosol Characterization Experiment (ACE 1): Aerosol Mass concentra-

tion and scattering and backscattering coefficients, *J. Geophys. Res.*, *103*(D13), 16,575–16,596.

Quinn, P. K., et al. (2005), Impact of particulate organic matter on the relative humidity dependence of light scattering: A simplified parameterization, *Geophys. Res. Lett.*, *32*, L22809, doi:10.1029/2005GL024322.

Quinn, P. K., et al. (2006), Impacts of sources and aging on submicrometer aerosol properties in the marine boundary layer across the Gulf of Maine, *J. Geophys. Res.*, *111*, D23S36, doi:10.1029/2006JD007582.

Raes, F., T. S. Bates, F. McGovern, and M. Van Liedekerke (2000), The 2nd Aerosol Characterization Experiment (ACE-2): General overview and main results, *Tellus*, *52*(2), 111–125.

Ramanathan, V., and A. M. Vogelmann (1997), Greenhouse effect, atmospheric solar absorption, and the Earth's radiation budget: From the Arrhenius-Langely era to the 1990's, *Ambio*, *26*(1), 38–46.

Ramanathan, V., P. J. Crutzen, J. T. Kiehl, and D. Rosenfeld (2001a), Atmosphere-aerosols, climate, and the hydrological cycle, *Science*, *294*(5549), 2119–2124.

Ramanathan, V., et al. (2001b), Indian Ocean Experiment (INDOEX): An integrated analysis of the climate forcing and effects of the great Indo-Asian haze, *J. Geophys. Res.*, *106*(D22), 28,371–28,398.

Redemann, J., P. B. Russell, and P. Hamill (2001), Dependence of aerosol light absorption and single scattering albedo on ambient relative humidity for sulfate aerosols with black carbon cores, *J. Geophys. Res.*, *106*, 27,485–27,495.

Rood, M. J., T. V. Larson, D. S. Covert, and N. C. Ahlquist (1985), Measurement of Laboratory and ambient aerosols with temperature and humidity controlled nephelometry, *Atmos. Environ.*, *19*(7), 1181–1190.

Rood, M. J., D. S. Covert, and T. V. Larson (1987a), Hygroscopic properties of atmospheric aerosol in Riverside, California, *Tellus, Ser. B*, *39*(4), 383–397.

Rood, M. J., D. S. Covert, and T. V. Larson (1987b), Temperature and humidity controlled nephelometry: Improvements and calibration, *Aerosol Sci. Technol.*, *71*(1), 57–65.

Rood, M. J., M. A. Shaw, T. V. Larson, and D. S. Covert (1989), Ubiquitous nature of ambient metastable aerosol, *Nature*, *337*(6207), 537–539.

Rosenfeld, D. (2000), Suppression of rain and snow by urban and industrial air pollution, *Science*, *287*, 1793–1796.

Ruby, M. G., M. J. Rood, A. P. Waggoner, E. Robinson, D. L. Blumenthal, and J. G. Watson (1989), Method 503: Integrating nephelometer measurement of scattering coefficient and fine particle concentrations, in *Methods of Air Sampling and Analysis*, 3rd ed., edited by J. P. Lodge Jr., pp. 450–457, Lewis Publ., Chelsea, Mich.

Russell, P. B., et al. (1999a), Aerosol-induced radiative flux changes off the United States mid-Atlantic coast: Comparison of values calculated from Sun photometer and in situ data with those measured by airborne pyranometer, *J. Geophys. Res.*, *104*, 2289–2307.

Russell, P. B., P. V. Hobbs, and L. L. Stowe (1999b), Aerosol properties and radiative effects in the United States East Coast Haze Plume: An overview of the Tropospheric Aerosol Radiative Observational Experiment (TARFOX), *J. Geophys. Res.*, *104*(D2), 2213–2222.

Russell, P. B., et al. (2002), Comparison of aerosol single scattering albedos derived by diverse techniques in two North Atlantic experiments, *J. Atmos. Sci.*, *59*(3), 609–619.

Saxena, P., and L. M. Hildemann (1996), Water-soluble organics in atmospheric particles: A critical review of the literature and application of thermodynamics to identify candidate compounds, *J. Atmos. Chem.*, *24*, 57–109.

Sempere, R., and K. Kawamura (1994), Comparative distributions of dicarboxylic acids and related polar compounds in snow, rain and aerosols from urban atmosphere, *Atmos. Environ.*, *28*, 449–459.

Shaw, M. A., and M. J. Rood (1990), Measurement of the crystallization humidities of ambient aerosol particles, *Atmos. Environ., Part A*, *24*(7), 1837–1841.

Sheridan, P. J., and J. A. Ogren (1999), Observations of the vertical and regional variability of aerosol optical properties over central and eastern North America, *J. Geophys. Res.*, *104*, 16,793–16,805.

Svenningsson, B., et al. (2005), Hygroscopic growth and critical supersaturations for mixed aerosol particles of inorganic and organic compounds of atmospheric relevance, *Atmos. Chem. Phys. Disc.*, *5*, 2833–2877.

Swietlicki, E., et al. (1999), A closure study of sub-micrometer aerosol particle hygroscopic behavior, *Atmos. Res.*, *50*(3–4), 205–240.

Takemura, T., T. Nozawa, S. Emori, T. Y. Nakajima, and T. Nakajima (2005), Simulation of climate response to aerosol direct and indirect effects with aerosol transport-radiation model, *J. Geophys. Res.*, *110*, D02202, doi:10.1029/2004JD005029.

Tang, I. N. (1980), Deliquescence properties and particle size change of hygroscopic aerosols, in *Generation of Aerosols and Facilities for Exposure Experiments*, edited by K. Willeke, chap. 7, pp. 153–167, Elsevier, New York.

Tang, I. N. (1996), Chemical and size effects of hygroscopic aerosols on light scattering coefficients, *J. Geophys. Res.*, *101*(D14), 19,245–19,250.

Tang, I. N., and H. R. Munkelwitz (1993), Composition and temperature dependence of the deliquescence properties of hygroscopic aerosols, *Atmos. Environ., Part A*, *27*(4), 467–473.

Tang, I. N., K. H. Fung, D. G. Imre, and H. R. Munkelwitz (1995), Phase transformation and metastability of hygroscopic microparticles, *Aerosol Sci. Technol.*, *23*, 443–453.

ten Brink, H. M., A. Khlystov, G. P. A. Kos, T. Tuch, C. Roth, and W. Kreyling (2000), A high flow humidograph for testing the water uptake by ambient aerosol, *Atmos. Environ.*, *34*, 4291–4300.

Twomey, S. (1991), Aerosols, clouds and radiation, *Atmos. Environ., Part A*, *25*(11), 2435–2442.

Virkkula, A., N. C. Ahlquist, D. S. Covert, W. P. Arnott, P. J. Sheridan, P. K. Quinn, and D. J. Coffman (2005), Modification, calibration and a field test of an instrument for measuring light absorption by particles, *Aerosol Sci. Technol.*, *39*, 68–83.

Weiss, R. E., T. V. Larson, and A. P. Waggoner (1983), In-situ rapid response measurement of $H_2SO_4/(NH_4)_2SO_4$ aerosols in rural Virginia, *Environ. Sci. Technol.*, *16*, 525–532.

Wiscombe, W. J., and G. W. Grams (1976), The backscattered fraction in two-stream approximations, *J. Atmos. Sci.*, *33*, 2440–2451.

T. S. Bates and P. K. Quinn, Pacific Marine Environmental Laboratory, NOAA, Seattle, WA 98115, USA.

C. M. Carrico, Department of Atmospheric Science, Colorado State University, Fort Collins, CO 80523, USA.

D. S. Covert, Department of Atmospheric Sciences, University of Washington, Seattle, WA 98195, USA.

M. J. Rood (corresponding author) and W. Wang, Department of Civil and Environmental Engineering, University of Illinois, 205 N. Mathews Avenue, Urbana, IL 61801, USA. (mrood@uiuc.edu)